CHALMERS
UNIVERSITY OF TECHNOLOGY

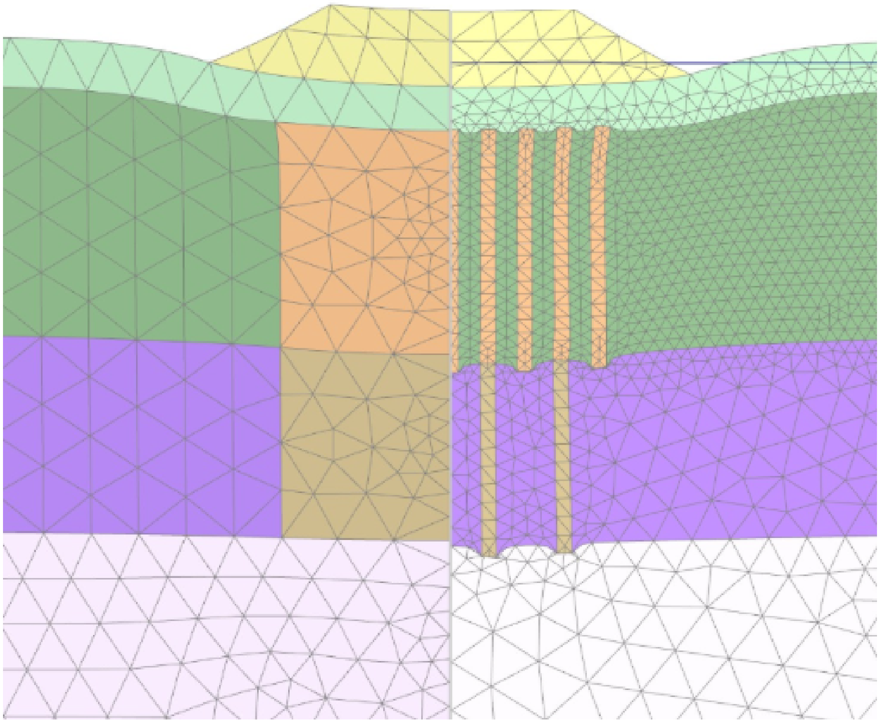

Numerical Modeling of Lime-Cement Columns Using PLAXIS 2D and 3D

Master's thesis in Architecture and Civil Engineering

Kiana Farmanesh, Tomas Överström

DEPARTMENT OF Infrastructure and Environmental Engineering

CHALMERS UNIVERSITY OF TECHNOLOGY
Gothenburg, Sweden 2026
www.chalmers.se

Master's thesis 2026

Numerical Modeling of Lime-Cement Columns Using PLAXIS 2D and 3D

Kiana Farmanesh
Tomas Överström

CHALMERS
UNIVERSITY OF TECHNOLOGY

Department of Infrastructure and Environmental Engineering
Division of Geology and Geotechnics
Chalmers University of Technology
Gothenburg, Sweden 2026

Numerical Modeling of Lime-Cement Columns Using PLAXIS 2D and 3D
KIANA FARMANESH, TOMAS ÖVERSTRÖM

Supervisor: Ayman Abed, Associate Professor - Division of Geology and Geotechnics
Supervisor: Anders Kullingsjö, Skanska
Examiner: Ayman Abed, Associate Professor - Division of Geology and Geotechnics

Master's Thesis 2026
Department of Infrastructure and Environmental Engineering
Division of Geology and Geotechnics
Chalmers University of Technology
SE-412 96 Gothenburg
Telephone +46 31 772 1000

Cover: Deformed Mesh of Embankment and Lime-Cement Columns as Visualized Using VAT (left), and 3D (right).

Typeset in LaTeX
Printed by Chalmers Reproservice
Gothenburg, Sweden 2026

Numerical Modeling of Lime-Cement Columns Using PLAXIS 2D and 3D
KIANA FARMANESH, TOMAS ÖVERSTRÖM
Department of Infrastructure and Environmental Engineering
Chalmers University of Technology

Abstract

This thesis investigated numerical modeling of lime–cement column (LCC) reinforced embankments using PLAXIS 2D and PLAXIS 3D. For 2D, the Volume Averaging Technique (VAT) which is a homogenization method was used, in which the soil was modeled using S-CLAY1S and the columns using the MNHard model. The aim was to evaluate VAT in PLAXIS 2D for reproducing the behavior of the Nödinge test embankment with focus on Serviceability Limit State (SLS). In addition, two simplified 3D analyses were conducted. One using the same material models as in the VAT for comparison between 2D and 3D and the other using the Concrete Model for the columns to assess alternative, potentially less conservative modeling approaches.

The study confirmed that the VAT is a practical and sufficiently accurate tool for serviceability analyses of LCC-reinforced embankments. This due to its efficiency, advanced constitutive models, and reliable settlement and pore pressure response. 3D simulations captured transition zone and arching effects which was not included in VAT. Besides this variation the comparison of the VAT and 3D revealed that VAT is a simplification of a 3D problem in a 2D plane-strain model, but still with a very close accuracy.

For column models, MNHard gave more stable and realistic settlements, while the Concrete Model produced more conservative larger settlements due to its drainage type limitations. The concrete model however showed a high potential for capturing additional column behaviors and failure mechanisms making it potentially interesting for Ultimate Limit State analysis (ULS).

A limitation of this thesis was the lack of comprehensive laboratory data for calibrating the input parameters required for the numerical models. In addition, the comparison between column models was limited by the lack of measured settlement data, making it difficult to evaluate the accuracy of the Concrete Model.

Suggestions for further work include strengthening the link between VAT and the Swedish method, analyzing deformation mechanisms, exploring VAT for ULS, improving the Concrete Model for LCC columns, and including creep effects for floating columns.

Keywords: Volume Averaging Technique (VAT), PLAXIS, lime–cement columns, S-CLAY1S, MNHard, Concrete Model, Serviceability Limit State (SLS), Ultimate Limit State (ULS), transition zone, Swedish design method.

Acknowledgments

This thesis was carried out in spring 2026 as part of the Master's programme in Infrastructure and Environmental Engineering at Chalmers University of Technology. The project was conducted in collaboration with Skanska Teknik.

First and foremost, we would like to express our sincere gratitude to our supervisor and examiner, Ayman Abed, Associate Professor in the Division of Geology and Geotechnics at Chalmers University of Technology, for his valuable guidance and constructive feedback throughout this thesis work. The Volume Averaging Technique and the modeling conducted in PLAXIS was made possible through his support and expertise.

We would also like to thank our supervisor Anders Kullingsjö at Skanska for introducing us to the subject, providing valuable data, as well as help with the 3D modeling, giving us the opportunity to conduct this study.

We will also express our thanks to Skanska Sverige AB for providing us a license to use PLAXIS 3D Advanced, without which, this study would simply not be possible.

Finally, we would like to thank Torbjörn Edstam and Mats Karlsson for sharing their experience and knowledge of the reference project, and for providing valuable insights during the course of this work.

Kiana Farmanesh & Tomas Överström, Gothenburg, June 2026

List of Acronyms

Below is the list of acronyms that have been used throughout this thesis listed in alphabetical order:

CRS	Constant Rate of Strain
DA	Design Approach
DDM	Dry Deep Mixing
LCC	Lime-Cement Columns
MCC	Modified Cam Clay
MNHard	Matsuoka-Nakai Hardening Model
OCR	Over-Consolidation Ratio
POP	Pre-Overburden Pressure
S-CLAY1S	Anisotropic Soil Model with Bonding and Destructuration
SLS	Serviceability Limit State
UDM	User Defined Model
ULS	Ultimate Limit State
VAT	Volume Averaging Technique
WDM	Wet Deep Mixing

Nomenclature

Indices

$block$	Index for the stabilized composite block
col, c	Index for the lime-cement columns
eq	Index for the homogenized equivalent material
lim	Index for the borderline between plastic and elastic zones
$s, soil$	Index for the surrounding clay or soil
$v0, 0$	Index for initial or in-situ conditions

Greek Letters

α	Column area ratio (A_{col}/A_{total}) or initial yield surface inclination
β	Load distribution constant or relative effectiveness of rotational hardening
γ	Unit weight [kN/m^3]
δ, S	Settlement [m]
ϵ	Strain
η_{lc}	Load distribution factor (Load Split)
κ	Swelling index
λ	Compression index
μ, ω	Absolute effectiveness of rotational hardening
μ_{zB}, μ_{zL}	Depth-reduction factors for stress distribution
ν	Poisson's ratio
ξ	Absolute rate of destructuration
σ'	Effective stress [kPa]
σ'_c	Pre-consolidation pressure [kPa]
ϕ'	Effective friction angle [°]
ψ	Dilatancy angle [°]
Ω_c, Ω_s	Volume fractions of columns and soil in VAT

Roman Letters

B, L	Width and length of the embankment $[m]$
c'	Effective cohesion $[kPa]$
c'_{col}	Cohesion intercept for the columns $[kPa]$
$c_{u,col}$	Undrained shear strength of columns $[kPa]$
C_v	Coefficient of consolidation $[m^2/s]$
d	Diameter of the columns $[m]$
D, H	Column length or total depth to firm layer $[m]$
D_{eq}	Equivalent stiffness matrix for homogenized material
E_{50}	Confining stress dependent stiffness modulus $[MPa]$
E_{col}, E_{28}	Column stiffness (Young's modulus) $[MPa]$
f_{lcc}	Compression strength in the columns $[kPa]$
$f_{c,28}$	Uniaxial compressive strength after 28 days $[kPa]$
G_{ref}	Reference shear modulus $[MPa]$
I_B, I_L	Geometrical factors of influence for stress spreading
k	Permeability / Hydraulic conductivity $[m/s$ or $m/day]$
m	Power of hyperbolic stress-strain law
M_0	Initial compression modulus $[kPa]$
M_L	Compression modulus in the linear range $[kPa]$
M_{block}	Representative modulus for the stabilized block $[MPa]$
M_{soil}	Representative modulus for the surrounding soil $[MPa]$
p_{ref}	Reference pressure (usually 100 kPa)
$P_{failure}$	Short-term failure load of an individual column $[kN]$
q	Embankment surface load $[kPa]$
R_f	Failure ratio
s	Center-to-center spacing of columns $[m]$
T_v	Time factor for consolidation
U_v	Degree of consolidation
z_{lim}	Limit depth of the plastic zone $[m]$

Contents

List of Acronyms **ix**

Nomenclature **xi**

List of Figures **xv**

List of Tables **xix**

1 Introduction **1**
1.1 Background 1
1.2 Aim 2
1.3 Limitations 3
1.4 Method Overview 4
1.5 Social, Ethical and Ecological Impacts 4

2 Reference Project **5**
2.1 Report 15 5
2.2 Site Characterization 5
2.3 Column Properties 8

3 Hand Calculated Settlements **10**
3.1 Green Field Settlements 13
3.2 Settlements for LCC-reinforced Soil, excluding Creep 15
3.2.1 Additional Stresses 16
3.2.2 Effective Vertical Stress Increment 18
3.2.3 Elastic-Plastic Zones 20
3.3 Consolidation Settlements 23
3.3.1 Creep Settlements 27
3.4 Compression Strength in the Columns f_{lcc} 27

4 Material Models **29**
4.1 S-CLAY1S 29
4.1.1 Material Parameter 30
4.2 MNHard Model 32
4.2.1 Material Parameters 34
4.3 Volume Averaging Technique 36
4.4 Concrete Material Model 37

4.4.1 Material Parameters . . . 38
4.5 Soil Test Calibration . . . 41

5 Simulation **45**
5.1 Geometry 2D . . . 45
5.2 Geometry 3D . . . 46
5.2.1 Mesh Sensitivity Analysis . . . 47
5.3 Permeability Sensitivity Analysis . . . 48
5.4 Impact of Excess Pore Water Pressure . . . 49
5.5 Problems Encountered During Simulations . . . 50
5.5.1 Problems in 2D . . . 50
5.5.2 Problems in 3D . . . 51

6 Results **52**
6.1 Settlements . . . 52
6.2 VAT Validation . . . 53
6.3 3D MNHard Validation [Type A] . . . 55
6.4 Concrete Model Validation [Type A] . . . 57
6.5 Comparison of Constitutive Models . . . 58
6.6 Excess Pore Water Pressure . . . 60

7 Discussion **62**
7.1 Reliability of Material Parameters . . . 62
7.2 Concrete Model . . . 63
7.3 VAT vs 3D Modeling . . . 64
7.3.1 Comparison of the Constitutive Models . . . 65
7.4 Pore Pressure Behavior . . . 65
7.5 Creep . . . 66
7.5.1 Differential Settlements . . . 66
7.6 Numerical Stability and Modeling Limitations . . . 66

8 Conclusion **68**
8.1 Volume Averaging technique (VAT) . . . 68
8.2 Comparison of Constitutive Models . . . 69
8.3 Suggestions for Further Work . . . 70

Bibliography **70**

A CRS Data **73**

B Creep Settlements **75**

C Material Parameters **77**

List of Figures

2.1 Constructed test embankment in Nödinge (Edstam, 2007) 6
2.2 Visualization of the site, including embankment and LC-columns. Characterized using available information from the report (Swedish Deep Stabilization Research Centre et al., 2006) 7

3.1 Visualization of the transition zone, where α is assumed to be 60° . . 11
3.2 Visualizing zone divisions (Not to scale) 12
3.3 Green Field effective stress distribution versus depth, The blue lines determine the different cases for settlement calculation following Swedish method 13
3.4 Settlements for the Green Field case 15
3.5 Load Split Model (Not to scale) 16
3.6 Column Area Ratio 17
3.7 Clays compression modulus vs. depth 20
3.8 Illustration showing the conceptual division between plasticity and elasticity 21
3.9 $\Delta\sigma_{blocklim}$ gives the stress increment at the limit between the two zones which is set to comparison with $\Delta\sigma_{block}$ as in the general expression for the stress increment 22
3.10 Illustration of the drainage paths for water in the underlying soil. The length of the arrows visualize the probability of the water molecule draining in either direction 25
3.11 Settlements over time for the stabilized block, the soil underneath, and the total settlements 26
3.12 Consolidation settlements from the report, compared to the hand-calculations 26

4.1 The yield surfaces for the S-CLAY1S model 30
4.2 Visual determination of the slope of the compression and swelling lines. 32
4.3 Matsuoka-Nakai (MN) and Mohr-Coulomb (MC) failure criterion in octahedral (Vogler, 2008) 33
4.4 The hyperbolic stress-strain relationship 34
4.5 Normalized stress-strain curve in compression (Seequent, 2025). 40
4.6 Replicating Type A MNHard parameters with the Concrete Model using Soil Test 42
4.7 Map showing the location of Nödinge and Löftaån, in relation to Gothenburg. Modified Map from Google Maps 43

4.8 Soil Test calibration in PLAXIS for both material models, compared to real Triaxial data [Type B](Baker, 2000) 43
4.9 Simulated Triaxial tests conducted on Type A and B parameters for both material models, as well as the real triaxial data from (Baker, 2000) 44

5.1 Illustration of the 2D model 45
5.2 3D geometry of the Nödinge embankment 47
5.3 Graph showing the convergence from the mesh sensitivity analysis . . 48
5.4 Permeability Sensitivity Analysis conducted on the VAT model (left), and the 3D MNHard model (right) 49

6.1 The hand calculated settlement compared to the real settlement data 52
6.2 The simulated settlements using VAT, compared to the real settlement data 53
6.3 Settlements versus depth measured inside an LC column (NbsCp18) and in the surrounding soil (NbsCl37) (Swedish Deep Stabilization Research Centre et al., 2006), compared with VAT simulations 379 days after final construction 54
6.4 The settlement of the soil between the columns, for every depth at multiple points in time, compared with the VAT simulation 54
6.5 The simulated settlements using MNHard model in 3D [Type A], compared to real settlement data 55
6.6 The simulated settlements using VAT and MNHard in 3D [Type A] . 56
6.7 Settlement over depth from 3D analysis and VAT, showing close agreement between the two simulations 56
6.8 The simulated settlements using Concrete Model in 3D [Type A], utilizing both available drainage formulations, compared to real settlement data 57
6.9 Comparison of the Concrete and MNHard constitutive models utilizing Type B parameters and the drained formulation 58
6.10 Comparison of the Concrete and MNHard constitutive models utilizing Type B parameters and the non-porous formulation 59
6.11 Comparing the impact of the drainage formulation for the MNHard model 59
6.12 Comparing the impact of the drainage formulation for the Concrete Model 60
6.13 Excess Pore Pressures over time in column at 14 meters depth 61

A.1 Data extracted from provided CRS test at 10 meters depth 73
A.2 Data extracted from provided CRS test at 15 meters depth 73
A.3 Data extracted from provided CRS test at 21 meters depth 74
A.4 Data extracted from provided CRS test at 27 meters depth 74
A.5 Results of triaxial compression test at 20 kpa confining pressure (Baker, 2000) 74

B.1 Calculated creep settlements for the stabilized block 75

B.2 Calculated creep settlements for the underlying clay 76

List of Tables

2.1 Nödinge Site-Specific Parameters. Z being depth below the surface in meters (Swedish Deep Stabilization Research Centre et al., 2006) . 8
2.2 Column parameters for LC-columns in Nödinge (Swedish Deep Stabilization Research Centre & Larsson, 2006) 9

3.1 Zonation of the soil-column system 12
3.2 Calculated settlements at different depth intervals 14
3.3 Comparison of calculated settlements for different depth intervals . . 23
3.4 Consolidation, creep, and total settlements for the block and soil after 24 years 27
3.5 The short-term failure load of the columns vs. depth 28

4.1 List over required material parameters for S-CLAY1S Model 31
4.2 List of required material parameters for MNHard Model 35
4.3 List of required material parameters for the Concrete Model 39

5.1 The simulated construction phases following the same order as presented in report 15 (Swedish Deep Stabilization Research Centre et al., 2006) 46

C.1 Material Parameters for S-CLAY1S Model before Soil Test - Type A . 77
C.2 Material Parameters for S-CLAY1S Model After soil Test 77
C.3 Material Parameters for MNHard Model before Soil Test - Type A . . 78
C.4 Material Parameters for MNHard Model after Soil Test - Type B . . 78
C.5 Material Parameters for concrete Model - Type A 78
C.6 Material Parameters for concrete Model - Type B 79

1
Introduction

Due to increasing urbanization, the evaluation and development of ground improvement techniques have become increasingly important. Several methods exist, among which lime–cement columns (LC-columns) are commonly used in areas with poor soil conditions. This method has been used in Sweden since 1975 to improve stability and reduce settlements under road and railway embankments as well as for trenches and other infrastructure needs (Helen Åhnberg & Göran Holm, 1986). Despite its long history and widespread adoption, it remains a strong interest to further refine design methodologies, particularly to extend the use of columns to more demanding applications and to improve predictive models of soil–column interaction.

As the method has maintained its original concept over the years, there have been significant developments in its applications such as the use of new binders and higher strength levels. However, the behavior of columns and the soil–column interaction is still assessed in a rather conservative manner, as the same simulation and calculation models have been used throughout the development of this concept (Larsson Stefan, 2025). Therefore, it is necessary to optimize these calculations by developing a less conservative design model that can consider more critical deformation and failure mechanisms. This would save material and lead to a more efficient design, benefiting both the climate and technical performance.

1.1 Background

There are several methods available for soil improvement utilizing deep mixing. These methods are differentiated depending on the binder used as well as the method of mixing (Broms, 2004). The geological prerequisites and the site characterization, as well as the dimensioned load and limit state requirements dictate which of these methods are most viable in terms of stability, stiffness and overall effectiveness. Of these dimensioning parameters, the type of soil is the most important when determining which method to use, as the binder's effectiveness is heavily dependent on soil material, and water content (Carlsten & Swedish Geotechnical Institute, 1996).

In the Nordic region, especially in Sweden, lime and lime–cement columns have been widely applied as a ground improvement solution for weak or compressible soils such as soft clay, silt and organic soils (Broms, 2004).

This method is based on the principle of the mechanical mixing of the binding agents in the ground at regular intervals to create cylindrical columns (Jonsson, 2024). These binders can be pure lime, pure cement, or a mix of both. In addition to lime and/or cement, additives can be used if additional functions are desired, such as frost resistance, or to simply reduce the environmental impact by replacing some amount with a more environmentally friendly additive, such as fly ash or alternative binders based on industrial byproducts.

In Nordic region, the dry mixing method is particularly common due to the high natural water content of many soft clays (Broms, 2004). Dry binders react with the in-situ moisture and are blended with the soil during installation, producing columns with improved strength and stiffness. This flexibility in installation and adaptation to local soil conditions has contributed to the method's popularity in Sweden, Norway, and Finland (Broms, 2004).

Depending on the desired outcome of the ground stabilization, such as slope stability or minimizing differential settlements, these LC-columns can be arranged in different ways. The most basic form is the triangular or square single-column pattern which is used when the main purpose of the ground improvement is the reduction of settlements (Vogler, 2008). If the main purpose instead lies in the stability of slopes, embankments or other structures, these columns can be installed in overlapping patterns, where the shape, alignment, and pattern, are placed where the shear stress is highest (Broms, 2004).

The concept with LC-columns is that the stability, and settlement magnitude is improved by transferring most of the load to the columns, which have a much higher stiffness than the surrounding soil. The columns initially take up the major part of the load and later transfer a reduced portion of it to the underlying soil (Jonsson, 2024). In this way, the load carried by the soil is reduced and redistributed more evenly, leading to lower stresses in the surrounding soil and minimized settlements (Jonsson, 2024).

In traditional hand calculations, the load distribution and column-soil interaction is determined by available guidelines and standards around the world which somewhat follow a similar base of assumption (Alén, 2009) (European Committee For Standardization, 2004). Where traditional hand calculations become limited, numerical modelling offers the possibility to capture more advanced soil-structure interaction mechanisms in either two or three dimensions, by utilizing advanced constitutive material models (Becker & Karstunen, 2014). These numerical approaches allow for a more accurate prediction of the soil's behavior after being improved by LC-columns.

1.2 Aim

The aim of this thesis is to evaluate how well the proposed numerical modeling approach, the Volume Averaging Technique (VAT) in PLAXIS 2D, captures the real settlements and Serviceability Limit State (Abed, Vogler, & Karstunen, 2026) in an embankment case compared to observed field measurements. In addition to the 2D simulation, two simplified three-dimensional analyses will be conducted, in order to assess the accuracy of the VAT approach in PLAXIS 2D compared with equivalent material models in 3D, with respect to field measurements.

In addition, due to the interest in new material models for the columns, the concrete model is implemented in the selected simulation configuration and compared with the existing alternatives. The aim is to assess whether the new column model captures a more accurate representation of the soil settlement response. This is achieved by capturing additional deformation mechanisms, thereby providing a less conservative and more accurate result.

1.3 Limitations

This section discusses the limitations associated with this thesis which depends on the assumptions and simplifications made during the study.

A limitation with the models was keeping the reference material and input material data consistent between the column models. In the thesis, two types of input parameters are introduced, where one of them took reinforcement from another test field's laboratory data, which later revealed that the results did not have the same properties as the desired column in the reference project. Therefore the comparison between the column models can not be used to assess whether one is more realistic or conservative.

For the chosen material models themselves, one major limitation for the comparison between material models in 3D is the fact that the Concrete Model can not simulate undrained behavior, which is the desired drainage type for settlement calculations with LC-columns. This limitation is slightly minimized by also comparing the MN-Hard simulation in drained and undrained calculation.

Another limitation is the neglect of creep in the simulations. This may partly explain some of the differences between simulated and measured results. It also leads to conservative predictions over longer time spans than considered in this thesis. In cases with floating columns, the underlying soil can exhibit significant creep settlements, which require appropriate models to capture. The omission of creep in the soil between columns was due to the incompatibility of the VAT formulation with creep models. It was also neglected in the underlying soil because of numerical difficulties arising from combining multiple complex material models.

In this thesis, the stability of the embankment and the system will not be evaluated or considered. This is due to VAT being solely focused on SLS applications, and thus not being able to conduct stability evaluations.

Lastly, the upper 2 meters are more or less disregarded in all simulations and calculations in the reference project. This is due to installation inefficiencies, where the shallow depths do not usually reach the desired stiffness and are therefore scraped away in practice. In the reference report, the first 2 meters were identified as such, and the settlement data was therefore also presented from -2 m onwards. The same assumption is made in this thesis, and the results from -2 m are used to ensure a fair comparison.

1.4 Method Overview

A reference project was selected as a source for most material parameters and real measured data that was used to validate the calculations and simulations. Initially, calculations following the Swedish Hand-calculation method were conducted. Afterwards, numerical simulations were conducted in PLAXIS 2D and 3D, utilizing the Volume Averaging Technique in 2D, as well as an additional constitutive model for the columns in 3D. The soil parameters were derived using CRS-data from the area accessed through Skanska archives, while the column parameters were derived using both data from the reference project, as well as data from triaxial compression tests from another location (Swedish Deep Stabilization Research Centre et al., 2006)(Baker, 2000). These parameter sets are named Type A and Type B, respectively. These methods as well as the reference project are explained more thoroughly in the following chapters.

1.5 Social, Ethical and Ecological Impacts

On the basis of the formulated aim for this thesis, improving simulation approaches so that the settlement responses for LC-columns beneath embankments can be represented as realistically as possible offers advantages from societal, environmental, and technical perspectives. As mentioned earlier, the design of LC-columns has largely remained based on the original concepts despite the developments through the years.

By increased environmental awareness and the high carbon emissions associated with cement and lime production, the interest in alternative, more sustainable binders have raised. Changes in binder composition affect both the strength and deformation behavior of the columns, as well as their interaction with the surrounding soil (Larsson Stefan, 2025). By enabling more advanced and flexible simulation methods, new environmentally friendly column designs can be evaluated and optimized without relying solely on conservative empirical assumptions. This contributes to sustainability by reducing material use, energy consumption, and design time, while improving the efficiency of the overall design and construction process.

From a societal perspective, more accurate simulations contribute to safer and more cost-effective infrastructure. Better predictions of performance reduce the risk of unexpected settlements or stability problems, which can otherwise lead to costly repairs, service disruptions, or safety hazards. In this way, improved modeling not only benefits the environment and engineering efficiency but also enhances the long-term reliability and resilience of infrastructure systems that society depends on.

2
Reference Project

During the period of 1996-2000 an investment was carried out in deep stabilization of soft soils with LC-columns requested by the authorities and the industry. The joint research program was coordinated by The Swedish Deep Stabilization Research Centre. Through this research program, a number of investigations and test embankments were conducted to challenge and expand the application range of LC-columns, as well as to optimize the underlying engineering methodology (Edstam Torbjörn & Swedish Deep Stabilization Research Centre, 1997). One of these studies was Report 15 which is chosen as the reference project for this thesis (Swedish Deep Stabilization Research Centre et al., 2006).

2.1 Report 15

Report 15 aimed to optimize and further develop the calculation model for settlements of embankments reinforced by LC-columns. The project was based on test embankments along National Road 45/Nordlänken which was constructed and monitored over a period of three years before being presented in June 2006. The research project was carried out in collaboration between the Department of Geotechnical Engineering at Chalmers University of Technology and the Swedish Geotechnical Institute (SGI). The project was funded by the Swedish Transport Administration (formerly the Swedish Road and Rail Administrations) and the Swedish Deep Stabilization Research Centre (Swedish Deep Stabilization Research Centre et al., 2006).

2.2 Site Characterization

In preparation for the expansion of Swedish National Road 45 and the Norge/Vänern Line railway through the Göta River valley, a road plan and a railway plan were developed within Ale Municipality. The ground conditions here consist mainly of deep clay deposits. A total of four test embankments spread out in the municipality were constructed, where some had the same geological subsoil while some varied somewhat (Swedish Deep Stabilization Research Centre et al., 2006). For this thesis, the test embankment constructed in Nödinge is chosen to be investigated due to its uniform clay stratigraphy and its varying column lengths. The test embankment is shown in Figure 2.1.

Figure 2.1: Constructed test embankment in Nödinge (Edstam, 2007)

The geometry of the embankment has a crest length of 26 m and a crest width of 13 m, and was constructed in two loading stages to a total height of 2.8 m, including the working platform for column installation. This geometry corresponds to a total surface load of 45 kPa. The side slopes are approximately 1:1.5 (Swedish Deep Stabilization Research Centre et al., 2006).

The column lengths consist of a combination of 12 m and 20 m columns, with a total of 153 columns in each area. A conceptual visualization of the site is seen in Figure 2.2. Settlements and pore pressures were monitored for approximately three years to document the behavior of the embankments, and these data play a crucial role in capturing the accuracy and robustness of the results achieved within this thesis. The settlements were monitored using bellow hose gauges covering areas both within and immediately outside the embankment fill, and pore pressure gauges were used to capture the pore pressure development in both the soil and the columns.

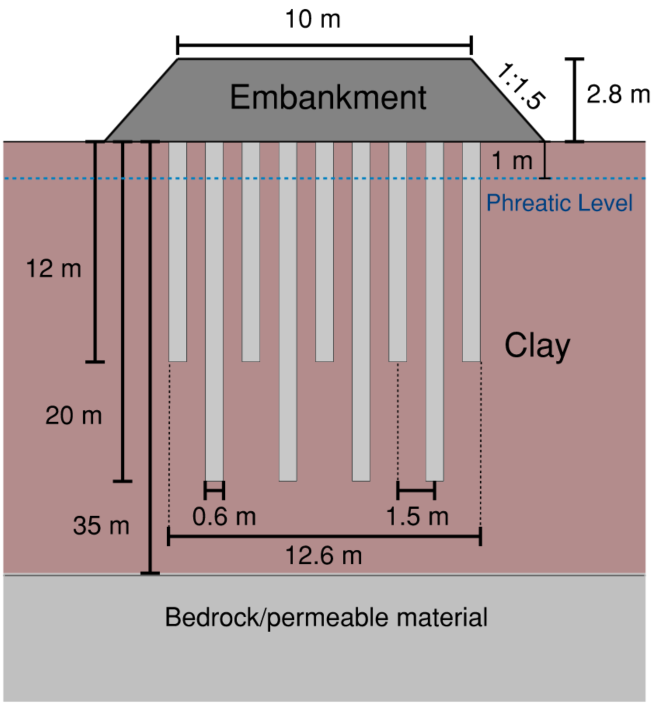

Figure 2.2: Visualization of the site, including embankment and LC-columns. Characterized using available information from the report (Swedish Deep Stabilization Research Centre et al., 2006)

To analyze the deformation resistance of the columns in the field, load tests and permeability tests were conducted. These were carried out on columns adjacent to Stora Viken, which is another test embankment than the one investigated in this report, but still considered relevant. The load tests were conducted as reversed column penetration tests (MOPS) for the end-bearing columns and as conventional top loading for the floating columns (Swedish Deep Stabilization Research Centre et al., 2006).

When it comes to the subsoil characterization in the area, the clay in Nödinge is slightly over-consolidated with an OCR of 1.2 and has a total thickness of 35 m before reaching a thin friction layer and bedrock/firm layer (Swedish Deep Stabilization Research Centre et al., 2006). At the surface there is a thin layer of dry crust which is ignored in the calculations due to the negligible thickness as well as high organic content as the investigations have revealed (Edstam, 2026). The groundwater level lies barely 1 m under the ground surface. The columns are designed with a diameter of 600 mm and are installed in a square grid with a fixed center-to-center distance of 1.5 m. The lengths, as mentioned earlier, vary, with the shorter ones being 12 m and the longer ones 20 m, all of them being floating columns. Test columns were installed, and soundings were carried out after 7, 14, and 28 days, evaluating a characteristic shear strength of 160 kPa after 30 days, excluding the first two meters due to insufficient strength in the columns at shallow depths (Swedish Deep Stabilization Research Centre et al., 2006).

In Table 2.1 The basic material properties are compiled using the processed results provided in the report, which were in turn obtained from a series of laboratory tests (Swedish Deep Stabilization Research Centre et al., 2006). However, since most of the raw laboratory and in-situ data were not available or presented, the validity of the parameters could not be independently assessed, and critical evaluation could not be applied. The parameters were therefore adopted directly, relying on the reported accuracy and correctness of the results.

In addition to the initial modulus - M_0 - and modulus in linear range - M_L - which was provided, the increment of the compression modulus - M' - was graphically determined using the provided CRS-test conducted on multiple depths and provided in Table 2.1 as well (WSP/BohusGeo, n.d.).

In the case of this thesis, there was multiple CRS-tests done on varying depths and locations on the soil, which was accessed through Skanska's archives (WSP/BohusGeo, n.d.). Some relevant depths judged by the authors were chosen to represent the Stratigraphy. These CRS-curves are provided in Chapter A in Appendix. In addition to M', these tests were used to calculate and validate the compression and swelling index of the soil at varying depths.

Table 2.1: Nödinge Site-Specific Parameters. Z being depth below the surface in meters (Swedish Deep Stabilization Research Centre et al., 2006)

Parameter	**Equation**	**Boundary**	**Unit**
Density	$\rho = 1.45 + 0.006 \cdot z$	$z < 15\,\mathrm{m}$	ton/m^3
	$\rho = 1.54 + 0.007 \cdot z$	$z \geq 15\,\mathrm{m}$	ton/m^3
Reference pore pressure	$u = 10 \cdot (1 + 0.03) \cdot (z - 0.8)$		kPa
Pre-consolidation pressure	$\sigma'_c = OCR \cdot \sigma'_0$	$\sigma'_{c,\min} = 25\,\mathrm{kPa}$	kPa
OCR	$OCR = 1.2$		–
Upper effective stress level	$\sigma'_L = 1.3 \cdot \sigma'_c$		kPa
Initial Modulus M0	$M_0 = 50 \cdot \sigma'_c$		kPa
Modulus in linear range ML	$M_L = 4 \cdot \sigma'_c$	Minimum $6 \cdot \sigma'_{c,\min}$	kPa
Increment of compression modulus M'	$M' \approx 13$		

2.3 Column Properties

The column properties are presented in Table 2.2. Although these parameters are sufficient for performing hand calculations following the Swedish standard, additional parameters are required for the constitutive models used in the numerical modeling. The Swedish standard assumes a constant column stiffness, for instance, while the chosen constitutive model in this thesis captures stiffness in a stress-dependent manner. How these models work and which behaviors they capture are introduced and presented in Chapter 4.

Table 2.2: Column parameters for LC-columns in Nödinge (Swedish Deep Stabilization Research Centre & Larsson, 2006)

Parameter	**Definition**	**Value**	**Unit**
E_{col}	Column stiffness	150	MPa
k_{col}	Column permeability	$50 \cdot k_{soil}$	m/s
c'	Column cohesion	75	kPa
φ'	Friction angle	35	[$\circ$]
ν'	Poisson's ratio	0.33	-

To obtain the required additional data, triaxial tests conducted by Sadek Baker were used (Baker, 2000). In this project, LC-columns at another test site were further investigated, with more laboratory data available describing their overall behavior (Baker, 2000). This test site is located elsewhere at Löftaån in which both the site conditions and column characteristics are most similar to the case of Nödinge. The used triaxial test is presented in Chapter A in Appendix.

3
Hand Calculated Settlements

This chapter presents the hand calculation procedure for estimating settlements which is commonly used in Sweden, known simply as the Swedish Method. The method will be covered in all its steps, while being applied to the studied case. Most of the Swedish calculation methods used today were developed and initiated through the reference project for this thesis, namely the test embankments for the E45/Nordlänken project. These reference reports include contributions from several researchers and engineers (Edstam Torbjörn & Swedish Deep Stabilization Research Centre, 1997; Swedish Deep Stabilization Research Centre & Larsson, 2006; Swedish Deep Stabilization Research Centre et al., 2006).
The order of operations for the hand-calculations are based on the calculations made in (Swedish Deep Stabilization Research Centre et al., 2006), as these are the reference calculations for this thesis. The calculations procedure is as listed below.

1. Compiling of material properties
2. Calculation of stress increments
3. Calculation of representative modulus and properties for stabilized block and underlying soil
4. Calculation of settlements of stabilized block considering consolidation, with and without creep
5. Calculation of settlements of underlying soil, considering consolidation, with and without creep

The settlement calculations are divided into two categories of the total settlement for the embankment without reinforcement, i.e. Green Field condition, and the settlement with LC columns.

The model developed by Clas Alén, Sadek Baker, Per-Evert Bentsson, and Göran Sällfors is followed (Alén et al., 2005). The method is based on dividing the soil under the embankment into three zones and a transition zone and thereby analyzing how the load is distributed between them, see Figure 3.2. This three-zone approach originates from the configuration of floating piles, which was relatively new at the time, and for which existing calculation methods were not sufficiently accurate (Alén et al., 2005).

The transition zone is the layer before the stresses fully develop into the LCC. This zone is governed by the arching occurring under the embankment, where one part of the load Q_1 is carried by the arching that form within the embankment, transferring pressure directly into the columns. The remaining load Q_2 is instead transferred through the soil and then into the columns via shear stresses along the perimeter, as the soft soil tries to settle past the stiffer columns. At the bottom of the transition load, the stiff columns have attracted the majority of the total stresses, and as such, the transition zone is the space required for the all the load to find the columns (Swedish Deep Stabilization Research Centre et al., 2006). This concept is visualized in Figure 3.1.

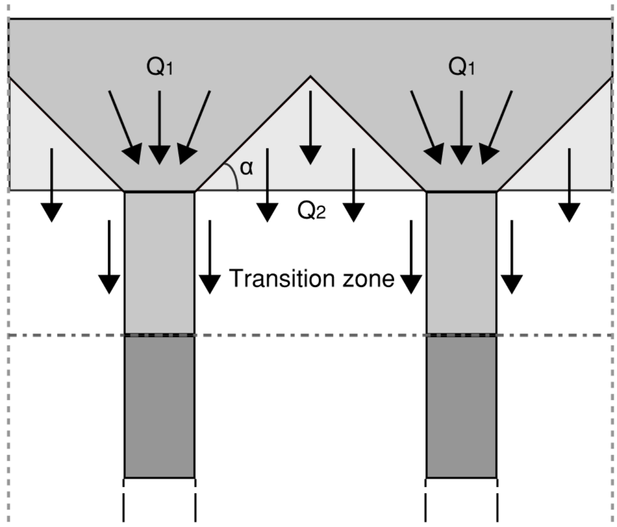

Figure 3.1: Visualization of the transition zone, where α is assumed to be 60°

A significant portion of the total settlement typically occurs in this zone, including differential settlements between the columns and the surrounding soil, which is primarily a serviceability - SLS - concern. However, under higher loads, the shear strength of the soil in this zone may be exceeded, making it relevant for ultimate limit state - ULS - considerations as well. On the other hand the transition zone between the embankment and the stabilized block can vary considerably due to installation effects and the quality of the upper columns. For these reasons, the transition zone is separated and analyzed independently (Swedish Deep Stabilization Research Centre et al., 2006).

In the reference project for capturing this zone a traditional hand-calculation is not applied and a new approach is introduced (Swedish Deep Stabilization Research Centre et al., 2006). In this thesis, the transition zone is not analyzed at the same level of detail. However, the reported results from the reference project are used as a basis for the adopted assumptions. According to the in-situ measurements of the columns compression strength, the considered arching effect, and the consideration of shear stress at the columns perimeter, the transition zone is assumed to extend to a depth of 2 meters in all calculations, and this assumption is therefore also used as a reference in the present thesis (Swedish Deep Stabilization Research Centre et al., 2006).

Beneath the transition zone lies the stabilized block. Due to the floating piles having varying lengths, this block is further divided into two zones, Zone A and Zone B, where the boundary between them corresponds to the depth at which the shorter piles end. The final zone, Zone C, consists of the underlying unstabilized soil, see Table 3.1 and Figure 3.2.

Table 3.1: Zonation of the soil-column system

Depth (m)	Zone	Description
2–12	A	Stabilized block consisting of both short and long LCC (Lime-Cement Columns).
12–20	B	Remaining length of the long LCC.
20–35	C	Underlying soil between the stabilized block and the firm layer/bedrock.

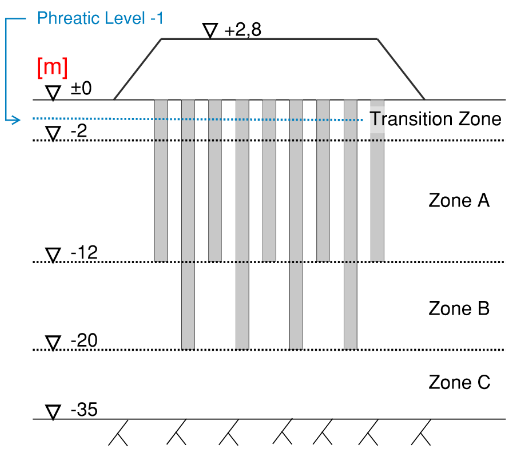

Figure 3.2: Visualizing zone divisions (Not to scale)

Some assumptions and simplifications are made throughout the suggested methodology in the reference project, which are important to keep in mind when comparing the results with the numerical modeling. These hand calculations only capture one-dimensional behavior through the depth of a cross section. This simplification affects the overall behavior of the system, particularly regarding water dissipation through the medium. This difference becomes important to have in mind when later comparing the results with 2D and 3D simulations.

Another simplification in the hand calculations is the neglect of loading phases. While the embankment was loaded in two stages, the hand calculations consider the loading as a single step. This mainly affects the visual appearance of the settlement curves, but it is not expected to significantly influence the magnitude of the long-term settlements.

3.1 Green Field Settlements

For the Green Field calculations the 2:1 method is conducted following the steps provided in (Sällfors, 2013) for both the total and consolidation settlements.

Given the applied load - q - of 45 kPa, the vertical total stress increment - $\Delta\sigma$ - is calculated by Equation 3.1. In this equation the width is adjusted given the slope of the embankment to 12 m and therefore used as width - b - in the hand-calculations.

$$\Delta\sigma_z = \frac{b \cdot q}{(b+z)} \tag{3.1}$$

From the equation above $\Delta\sigma$ decreases from 45 kPa at the ground surface to approximately 11.5 kPa at 35 m depth. The effective vertical stress σ'_0 is plotted in addition to the total vertical stress increment $\Delta\sigma'$ in relation to the pre-consolidation boundaries, thus Figure 3.3 is obtained.

Figure 3.3: Green Field effective stress distribution versus depth, The blue lines determine the different cases for settlement calculation following Swedish method

As the graph shows, the settlements at shallow depths exceed the upper limit of the pre-consolidation pressure, resulting in large settlements in these layers. The stresses gradually decrease with depth and transition to Case I, characterized by plastic deformations. According to the Swedish Method the settlements for these three cases are calculated following Equation 3.2 (Sällfors, 2013).

$$\delta = \begin{cases} \text{Case I:} & \sum h \dfrac{\Delta\sigma}{M_0} & \sigma'_0 + \Delta\sigma < \sigma'_c \\ \text{Case II:} & \sum h \left(\dfrac{\sigma'_c - \sigma'_0}{M_0} + \dfrac{\sigma'_0 + \Delta\sigma - \sigma'_c}{M_L} \right) & \sigma'_c < \sigma'_0 + \Delta\sigma < \sigma'_L \\ \text{Case III:} & \sum h \Bigg(\dfrac{\sigma'_c - \sigma'_0}{M_0} + \dfrac{\sigma'_L - \sigma'_c}{M_L} & \\ & \quad + \dfrac{1}{M'} \ln\left(1 + (\sigma'_0 + \Delta\sigma - \sigma'_L) \dfrac{M'}{M_L} \right) \Bigg) & \sigma'_0 + \Delta\sigma > \sigma'_L \end{cases} \tag{3.2}$$

Consequently the total settlements for the three cases and corresponding depths are presented in the Table 3.2.

Table 3.2: Calculated settlements at different depth intervals

Z [m]	**Settlements [m]**
0–9	1.22
9–17	0.2
17–35	0.31
Total	**1.74**

The plastic deformations (Case I) occurring in the first 9 meters account for the vast majority of the total settlements, providing ample evidence for the need to reduce the size of the plastic zone by utilizing ground improvement methods. Another important aspect in addition to the total settlements expected, is the rate of consolidation, which will be covered next.

Consolidation Settlements Green Field

To calculate the consolidation settlements a coefficient of consolidation - C_v - calculated by Equation 3.3 (Terzaghi, Peck, & Mesri, 1996), where k_v is the vertical permeability of the soil.

$$c_v = \frac{k_v}{\gamma_w \cdot m_v} \qquad m_v = \frac{1}{M} \tag{3.3}$$

As Figure 3.3 showed, the effective stress distribution passes the boundaries formed by the consolidation pressure therefore three different compression modulus of M_0 , M_L and M' are used, and an average C_v for the whole subsoil equal to $1.05{\times}10^{-7}\text{m}^2/\text{s}$ is calculated from the initial permeability of 10^{-9}m/s. This coefficient is then used to obtain time factor - T_v - from Equation 3.4, which is subsequently used to obtain the degree of consolidation - U_v - according to Equation 3.5 (Alén, 2012).

$$T_v = C_v \cdot \frac{t}{h^2} \tag{3.4}$$

$$U_v = \begin{cases} \sqrt{\dfrac{4T_v}{\pi}}, & T_v < 0.20 \\ U = 1 - 0.8 \cdot e^{-2.5 \cdot T_v} \end{cases} \tag{3.5}$$

The degree of consolidation shows how much of the total settlement is obtained for a given time t. For the Green Field case it is calculated to take approximately 160 years to reach the total settlements of 1.7 m, shown in Figure 3.4.

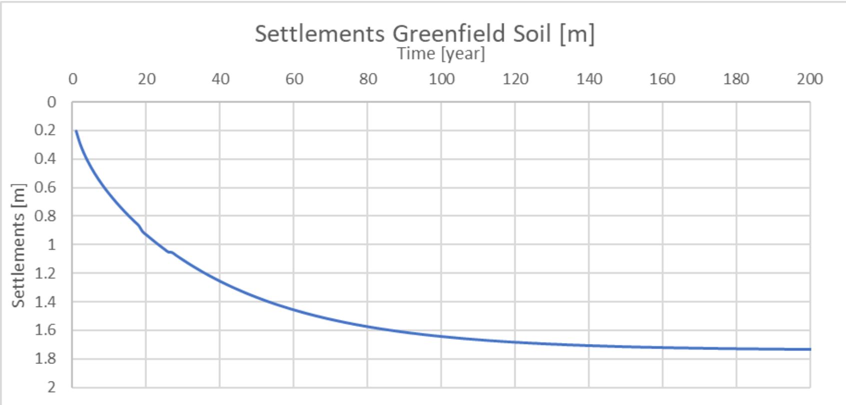

Figure 3.4: Settlements for the Green Field case

The rate of consolidation is as expected in a case of thick clay with low permeability without any measures to increase the effective permeability of the system. This shows why, in addition to limiting settlements by increasing system stiffness, there is a need to increase the rate of consolidation so the system reaches its maximum settlement in a reasonable amount of time.

3.2 Settlements for LCC-reinforced Soil, excluding Creep

For the reinforced soil with the LCC configuration a weighting of certain parameters is performed to obtain a representative value for the parameters to achieve a reliable but yet conservative settlement.

The whole layer is divided into two parts. The first is referred to as the block, including the properties of both the clay and the columns, and the second zone consists only of the underlying clay with its in-situ properties. The settlement for the underlying clay is calculated similarly to the Green Field case, while the block zone involves some additional steps. All the equations and procedure presented here are sourced from the Report 15 (Swedish Deep Stabilization Research Centre et al., 2006).

3.2.1 Additional Stresses

The initial vertical effective stress in the soil is the same as Green Field scenario but vertical effective stress increment - $\Delta\sigma'$ - is obtained differently since we have a composite material. The method that is used for the stress increment was proposed by the reference project of this thesis and still used today in the Swedish method.

In the previous assumption for LCC, the load distribution with depth caused by the surface load was neglected. While this assumption is acceptable for end bearing piles, it is considered too conservative for a floating configuration (Swedish Deep Stabilization Research Centre et al., 2006). Therefore, the load distribution is considered in two stages. One spreading from the surface, and another portion being transferred to the bottom of the block through the columns and subsequently distributed further into the underlying clay, as presented in Figure 3.5.

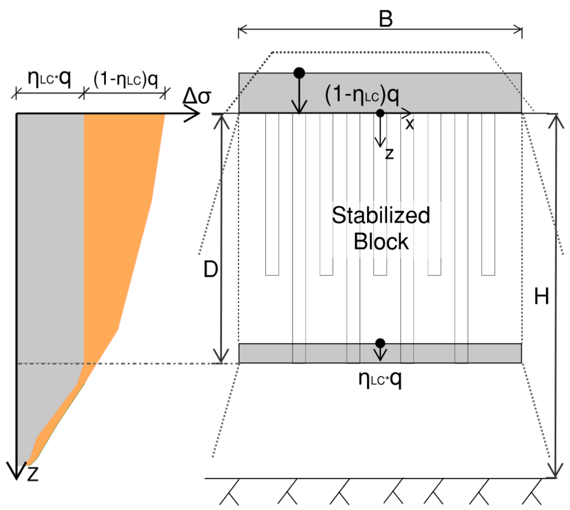

Figure 3.5: Load Split Model (Not to scale)

The proportion of the load that is distributed at the surface versus at the bottom of the block is determined by the load distribution factor - η_{lc} - and calculated by Equation 3.6 (Swedish Deep Stabilization Research Centre et al., 2006).

$$\eta_{lc} = (\frac{D}{H})^{\beta} \qquad \beta = \frac{1}{(\frac{M_{block}}{M_{soil}})^{\alpha} - (\frac{M_{soil}}{M_{block}})^{\alpha}} \tag{3.6}$$

η_{lc} depends on the modulus of the block, modulus of the soil, their ratio as well as the geometry as in depths of the composite material. This is an iterative process since the stiffness of the LC-columns and soil varies with depth. Physically, this means that for floating columns, this factor represents the efficiency of the columns in transferring load via shear stresses along their sides into the surrounding soil, compared to carrying it directly to the ends of the columns. The initial assumptions

for the ratio between the modulus of the block and soil are shown in Equation 3.7, which leads to $\eta_{lc} = 0.18$ (Swedish Deep Stabilization Research Centre et al., 2006)
.

$$\frac{M_{block}}{M_{soil}} = 5 \text{ and } a = 0,1 \tag{3.7}$$

To make sure about the validity of the assumption for the ratio between the block and soil modulus, these parameters are derived more in a formal manner. The representative compression modulus M needs to be determined for the soil - M_{soil} - and block - M_{block} - with respect to differing column lengths, see Figure 3.2. M_{soil} is calculated by Equation (3.8) to (3.10) (Swedish Deep Stabilization Research Centre et al., 2006).

$$M_{soil1} = \int_{2}^{12} M_0 \, dz = \int_{2}^{12} 50 \cdot \sigma_c' \, dz = 2{,}38 \, \text{MPa} \tag{3.8}$$

$$M_{soil2} = \int_{12}^{20} M_0 \, dz = \int_{12}^{20} 50 \cdot \sigma_c' \, dz = 5{,}27 \, \text{MPa} \tag{3.9}$$

$$M_{soil} = \frac{10 \cdot M_{soil1} + 8 \cdot M_{soil2}}{18} = 3.67 \text{ MPa} \tag{3.10}$$

Given the different lengths for the columns, two different column area ratios - α - as the ratio between the column area and the total influence area are calculated using Equation 3.11 (Sällfors & Alén, 2012). This formula is valid for a square grid pattern as visualized in Figure 3.6 (Baker, 2000).

$$\alpha = \frac{\pi d^2}{4 s^2} \tag{3.11}$$

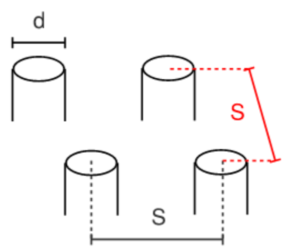

Figure 3.6: Column Area Ratio

With the chosen configurations the area factors $\alpha_1 = 0.13$ and $\alpha_2 = 0.065$ are obtained. Given the column stiffness $E_{col} = 150 \; Mpa$, M_{block} is calculated by Equation (3.12) to (3.14) (Swedish Deep Stabilization Research Centre et al., 2006).

$$M_{block1} = \alpha_1 \cdot E_{col} + (1 - \alpha_1) \cdot M_{soil1} = 20.9 \text{ MPa} \tag{3.12}$$

$$M_{block2} = \alpha_2 \cdot E_{col} + (1 - \alpha_2) \cdot M_{soil2} = 14.4 \text{ MPa} \tag{3.13}$$

$$M_{block} = \frac{10 \cdot M_{block1} + 8 \cdot M_{block2}}{18} = 18.01 \text{ MPa} \tag{3.14}$$

Thus the controlled fraction is 4.9 according to Equation 3.15, which is assumed close enough to the initial assumption, therefore no more iterations needed.

$$\frac{M_{block}}{M_{soil}} = 4.9 \tag{3.15}$$

3.2.2 Effective Vertical Stress Increment

The factor of influence is used to determine the geometrical spreading of stresses and can be described using Equation 3.16. This factor of influence represents the stress bulb effect, when the load moves deeper into the soil, the load spreads laterally into a larger volume and therefore dilutes with depth (Swedish Deep Stabilization Research Centre et al., 2006).

$$I(B,x,z) = \frac{1}{\pi}\left(\frac{2z(B+2x)}{4z^2+(B+2x)^2} + \text{atan}\left(\frac{B+2x}{2z}\right) + \frac{2z(B-2x)}{4z^2+(B-2x)^2} + \text{atan}\left(\frac{B-2x}{2z}\right)\right) \tag{3.16}$$

This equation refers to an infinitely long embankment with a finite width B. To approximate the spreading of stresses using the factor of influence for an embankment with finite geometry, the equation can be rewritten as Equation 3.17 (Swedish Deep Stabilization Research Centre et al., 2006).

$$\sigma_{3D}(q,B,L,x,y,z) = q * I(B,x,z) * I(L,y,z) \tag{3.17}$$

As the settlements are calculated in the middle of the embankment, x and y are both equal to zero, therefore the simplified factor of influence across width and length can be written as Equation 3.18 (Swedish Deep Stabilization Research Centre et al., 2006).

$$I_B(z) = \frac{2}{\pi}\cdot\left[\frac{6z}{z^2+36} + \text{atan}\left(\frac{6}{z}\right)\right] \text{ and } I_L(z) = \frac{2}{\pi}\cdot\left[\frac{12z}{z^2+144} + \text{atan}\left(\frac{12}{z}\right)\right] \tag{3.18}$$

The depth-reduction factor across - μ_{zB} - and along - μ_{zL} - the embankment need to be calculated using equations 3.19 and 3.20 to calculate the incremental stresses (Swedish Deep Stabilization Research Centre et al., 2006).

$$\mu_{zB} = 1 - 0.4\cdot\frac{B}{H} = 1 - 0.4\cdot\frac{12}{35} = 0.86 \tag{3.19}$$

$$\mu_{zZ} = 1 - 0.4\cdot\frac{L}{H} = 1 - 0.4\cdot\frac{24}{35} = 0.73 \tag{3.20}$$

Using the load distribution factor, the depth-reduction factor, and the factor of intensity provided in Equation (3.6) and (3.18) in addition to the initial load of 45 kPa, the incremental stresses can be calculated using Equation 3.21. Standard stress distribution models assume a "half-infinite" soil volume, but when a firm layer exists at a certain depth (H), it creates a physical boundary that causes stress concentration toward the center of the loaded area. These load distribution factors are a practical correction to account for the squeezing effect that appears when the soft clay encounters high stress at the top, and a hard boundary at the bottom (Swedish Deep Stabilization Research Centre et al., 2006).

$$\Delta\sigma_{LC}(z) = (1-\eta_{lc}) \cdot 45 \cdot I_B(\mu_{zB} \cdot z) \cdot I_L(\mu_{zZ} \cdot z) + \\ + \begin{cases} \eta_{lc} \cdot 45, & z < 20, \\ \eta_{lc} \cdot 45 \cdot I_B\Big(\mu_{zB} \cdot (z-20)\Big) \cdot I_L\Big(\mu_{zZ} \cdot (z-20)\Big), & z > 20 \end{cases} \tag{3.21}$$

From the total stress increment, the portion taken up by the soil can be determined using the compression modulus in the following Equation (3.22) and (3.23). The ratio of modulus M_{soil}/M_{block} is fundamentally based on the assumption of "plane sections remain plane", meaning an assumption that the bond between columns and soil are strong enough that they deform equally. As such, the columns take a higher share of the stress to maintain the strain equality with the soil (Swedish Deep Stabilization Research Centre et al., 2006).

$$\Delta\sigma'_{soil1}(z) = \frac{M_{soil1}}{M_{block2}} \cdot \Delta\sigma_{LC}(z) \tag{3.22}$$

$$\Delta\sigma'_{soil2}(z) = \frac{M_{soil2}}{M_{block2}} \cdot \Delta\sigma_{LC}(z) \tag{3.23}$$

For the settlement calculations, and for the sake of simplicity, instead of varying the compression modulus with depth and between cases, a representative modulus for the clay is defined as a function of depth and stress increment according to equation 3.24 (Swedish Deep Stabilization Research Centre et al., 2006).

$$M\Big(z, \Delta\sigma'_{\text{soil}}\Big) = \frac{\Big[\sigma'_L - \Big(\sigma'_0 + \Delta\sigma'_{\text{soil}}\Big)\Big] M_0(z) + \Delta\sigma'_{\text{soil}} \cdot M_L(z)}{\sigma'_L - \sigma'_0} \tag{3.24}$$

The new modulus for clay as well as M_0 and M_L are plotted in Figure 3.7 for the sake of comparison. As observed in the graph, the clay has its maximum compression strength at M_0 and its lowest at M_L. Based on the calculated surface load and the corresponding stress increment, the clay's compression modulus is obtained as illustrated by the yellow line in the figure. A representative value close to this is defined as 90% of M_0 and is therefore used in the settlement calculations (Swedish Deep Stabilization Research Centre et al., 2006).

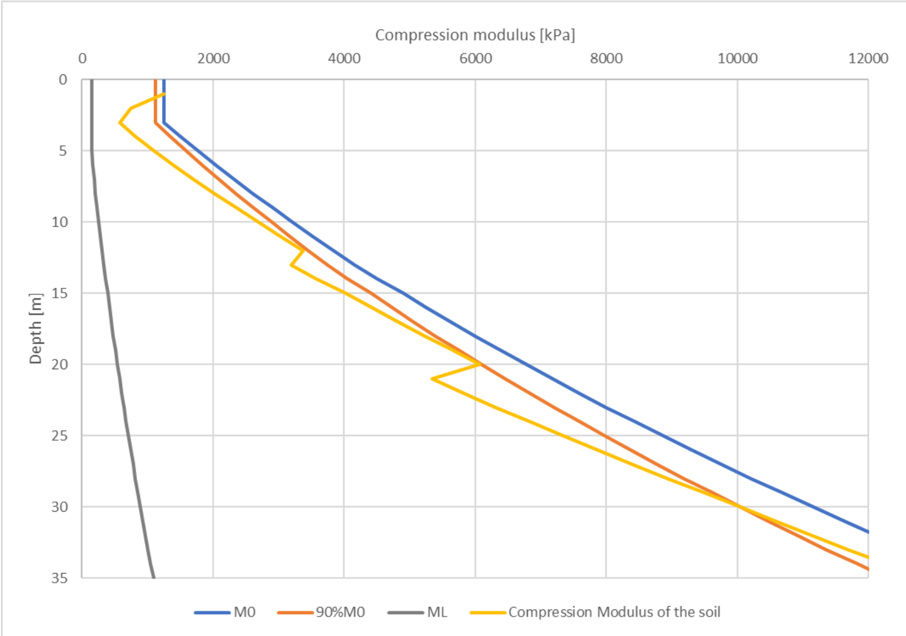

Figure 3.7: Clays compression modulus vs. depth

With the stress increments known both for the columns as well as the soil and with the representative modulus of each, the settlements are then calculated by Equation 3.25 (Swedish Deep Stabilization Research Centre et al., 2006).

$$\begin{aligned} S_{\text{block}} &= \int_{2}^{20} \frac{\Delta\sigma_{\text{soil}}(z)}{M(z,\Delta\sigma_{\text{soil}})}\,dz = 0.048\,\text{m} \\ S_{\text{soil}} &= \int_{20}^{35} \frac{\Delta\sigma_{Lc}(z)}{M(z,\Delta\sigma_{\text{Lc}})}\,dz = 0.023\,\text{m} \end{aligned} \tag{3.25}$$

3.2.3 Elastic-Plastic Zones

Even if the majority of this calculation method is the base for the Swedish standard today, some variations through the years are implemented and proposed. For comparison between the methods currently used and the one mentioned above and presented in the reference project, an additional approach is tested to examine whether similar results are obtained. The approach discussed in the following sections is presented by (Sällfors & Alén, 2012). For clarity's sake, the results for the method from Report 15 will be shown as Thesis I, while the second method will be shown as Thesis II.

For this method, a new concept is introduced in which a new zone division is defined. There is a "limit depth" in the columns where the soil column interaction is divided into a plastic and elastic response and thus the settlements calculation approach differs accordingly (Sällfors & Alén, 2012). This concept is illustrated in Figure 3.8.

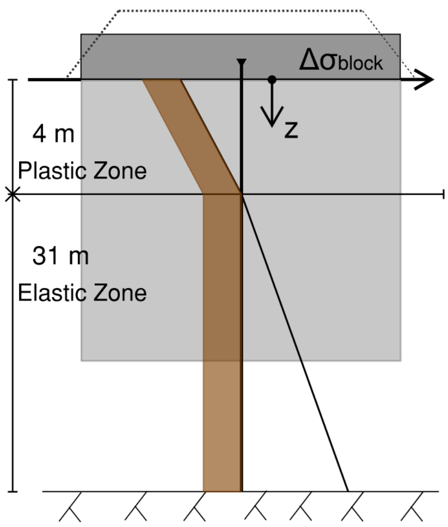

Figure 3.8: Illustration showing the conceptual division between plasticity and elasticity

The first zone is the plastic zone where the compression strength of the stabilized ground is insufficient compared to the applied load, and thus the columns are in the plastic failure state (Alén, 2009). In the elastic zone the columns are still intact and not plastically yielding (Sällfors & Alén, 2012). In the elastic zone the columns and the soil are considered to be completely interacted and therefore settlement calculations are carried out the same as Case I in Equation 3.2 where parameters for the block will instead be used (Sällfors & Alén, 2012). The extent of each zone and the borderline is determined using the relation found in Equation 3.26 (Alén, 2009):

$$\Delta\sigma_{block,lim} = \Delta\sigma_{block} \tag{3.26}$$

Where $\Delta\sigma_{block,lim}$ represents the stresses at $z = z_{lim}$ and $\Delta\sigma_{block}$ the stress increase at the border between the plastic and elastic zones. These are calculated by Equation 3.27 (Alén, 2009). $\Delta\sigma_{block,lim}$ is related to the compressive strength of the columns and is therefore governed by it.

$$\begin{aligned} \Delta\sigma_{\text{block,lim}} &= \frac{M_{\text{block}}\,(1.5\,C_{u,\text{col}} + \sigma'_{v0})}{E_{\text{col}} - 1.5\,M_{\text{soil}}} \\ \Delta\sigma_{\text{block}} &= \eta_{\text{Lc}}\,q + (1-\eta_{\text{Lc}})\,\frac{q\,B}{B+Z} \end{aligned} \tag{3.27}$$

After the zone division, the settlements can be calculated for each zone separately. For the plastic zone, the stress increase in the soil is calculated at the surface and at Z_{lim} using Equation 3.28. (Sällfors & Alén, 2012). This limiting depth divides the soil into the upper Zone A, where the compressive strength of the columns is insufficient to carry the elastic proportional part of the load, while in Zone B, the columns remain elastically intact. Thus allowing the columns and soil to be treated as a unified and stiff composite material (Alén, 2009).

$$\Delta\sigma_{\text{soil}}(0) = \frac{q - 3\,c_{u,\text{col}}}{2 + a}$$
$$\Delta\sigma_{\text{soil}}(Z_{\text{lim}}) = \frac{\Delta\sigma_{\text{block}}(Z_{\text{lim}})\,M_{\text{soil}}}{M_{\text{block}}} \tag{3.28}$$

Later for the plastic zone an average of the stress increase through Equation 3.29 can be conducted.

$$\Delta\sigma_{soil} = \frac{\Delta\sigma_{\text{soil}}(0) + \Delta\sigma_{\text{soil}}(Z_{lim})}{2}. \tag{3.29}$$

For the underlying clay on the other hand the stress increase is calculated differently by following Equation 3.30 and is used for settlement calculations from 20-35 m.

$$\Delta\sigma_{soil} = \frac{\eta_{LC} \cdot q \cdot B}{(B + (Z - D))} + \frac{(1 - \eta_{LC}) \cdot q \cdot B}{(B + Z)} \tag{3.30}$$

In this case the equilibrium in Equation 3.26 is reached at the depth of 4 meters, this is also visualized in Figure 3.9.

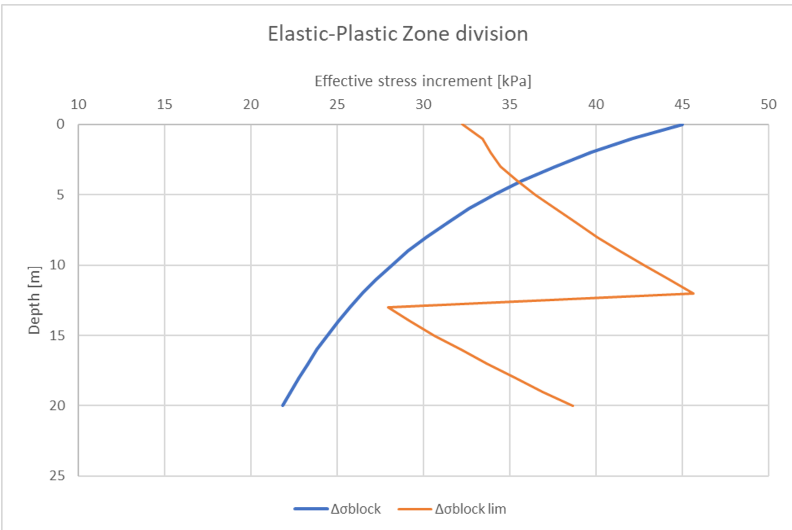

Figure 3.9: $\Delta\sigma_{blocklim}$ gives the stress increment at the limit between the two zones which is set to comparison with $\Delta\sigma_{block}$ as in the general expression for the stress increment

The settlements are then calculated as earlier but yet provided in detail in Equation 3.31.

$$S_{soil}(Z = 4) = \frac{\Delta\sigma_{soil} \cdot Z_{lim}}{M_{soil}} = 0.018\,\text{m} \tag{3.31}$$

For the elastic zone, the same concept is used and the detailed equations are provided in Equation 3.32.

$$S_{\text{block}} = \int_{4}^{20} \frac{\Delta\sigma_{\text{block}}(z)}{M_{block}}\,dz = 0.024\,\text{m}$$
$$S_{\text{soil}} = \int_{20}^{35} \frac{\Delta\sigma_{\text{soil}}(z)}{M_{soil}}\,dz = 0.026\,\text{m} \tag{3.32}$$

The results of the total settlements excluding creep from both calculations methods are summarized and presented in Table 3.3 for comparisons sake.

Table 3.3: Comparison of calculated settlements for different depth intervals

$z[m]$	Report 15	Thesis I	Thesis II	Green Field
2–20	0.038	0.049	0.041	
20–35	0.028	0.023	0.026	
Total [m]	0.066	0.072	0.067	1.74

The first column in the table presents the results obtained in the hand-calculations in the reference project. The second column shows the results achieved in this thesis when following the methodology presented therein, and the third column presents the results obtained by applying the Swedish method. As observed, all results are relatively close and similar, and the slight differences are due to rounding in the calculation process and the use of averaged parameters.

This resulting zonation represents a practical approximation for separating regions assumed to behave elastically and plastically beneath the embankment. It should however be noted that the Swedish zonation method is semi-empirical in nature, as the limiting depth is derived from simplified stress distribution assumptions and calibrated engineering practice, rather than being entirely derived based on rigorous scientific theory. The semi-empirical nature of this zonation motivates a later comparison with finite element simulations, where the developments of elastic and plastic behavior is directly derived from the constitutive models' numerical response.

3.3 Consolidation Settlements

In addition to reducing the total settlement magnitude, another benefit of utilizing LC-columns is to limit the amount of time for the total settlements to occur. To calculate the consolidation settlements, representative values for block and soil are calculated as these consolidation calculations are made separately. A mean value for block and soil modulus can be calculated following Equation 3.33. q_{block} and q_{soil} are the consolidation pressure i.e. the initial excess pore pressure in the system. These are calculated as an arithmetic mean value of the incremental stresses over the depth for block and soil respectively through Equation 3.34.

$$\begin{aligned} M_{block} &= \frac{q_{block}}{s_{block}} \cdot (D - 2m) = \frac{31,1}{0,048} \cdot 18 = 16,2\,\text{MPa} \\ M_{soil} &= \frac{q_{soil}}{s_{soil}} \cdot (H - D) = \frac{13.5}{0,023} \cdot 15 = 7.9\,\text{MPa} \end{aligned} \tag{3.33}$$

$$q_{block} = \int_{2}^{20} \frac{\Delta\sigma_{LC}(z)}{18} dz = 31.1 \text{ kPa and } q_{soil} = \int_{20}^{35} \frac{\Delta\sigma_{LC}(z)}{15} dz = 13.5 \text{ kPa} \tag{3.34}$$

Since now the properties of the block is averaged for both materials the same approach is used for the permeability properties. The representative permeability for the soil is calculated as a function of the strain, using Equation (3.35) to (3.37) below in unison. The equation for the change in permeability due to strain (equation 3.35) was determined using data from CRS-tests, calibrated and presented in the reference project (Swedish Deep Stabilization Research Centre et al., 2006).

$$k_\epsilon(\epsilon) = 10^{-(9+10\epsilon/3)} \Rightarrow k(z, \Delta\sigma') = 10^{-c} \tag{3.35}$$

$$c = 9 + \frac{10}{3}\frac{\sigma'_0 + \Delta\sigma'}{M(z, \Delta\sigma')} \tag{3.36}$$

$$k_0(z) = k(z, 0) \text{ and } k_L(z) = k(z, \sigma'_L - \sigma'_0) \tag{3.37}$$

A representative value for the soil permeability in the block and underlain soil is determined using integration following Equation 3.38.

$$\begin{aligned} k_{soil(block)} &= \int_2^{20} \frac{k(z, \Delta\sigma'/2)}{18} dz = 8.96 \cdot 10^{-10} m/s \text{ and} \\ k_{soil} &= \int_{20}^{35} \frac{k(z, \Delta\sigma'/2)}{15} dz = 8.62 \cdot 10^{-10} m/s \end{aligned} \tag{3.38}$$

In LCC stabilized soil, the columns act as vertical drains. Because columns are stiffer than the surrounding soil, they initially attract very high pore pressures which then dissipate through the columns. Traditional methods often use fictive permeability values to compensate the fact that the soil's inherent stiffness was underestimated. As such, k_{block} is more of a system property that describes how fast the entire system can dissipate pore pressures. To calculate the representative permeability for the LC-block as a composite material, the equation is weighted due to the columns area factor at differing depths, as well as with the assumption that $k_{col}/k_{soil} = 50$ (Swedish Deep Stabilization Research Centre et al., 2006).

$$\begin{aligned} k_{\text{block}} &= \frac{10[\alpha_1 \cdot 50 + (1-\alpha_1)] + 8\,[\alpha_2 \cdot 50 + (1-\alpha_2)]}{18} k_{\text{soil(block)}} = \\ &= \frac{10[0.13 \cdot 50 + 0.87] + 8[0{,}063 \cdot 50 + 0.935]}{18} \cdot 8.96 \times 10^{-10} = 5.19 \times 10^{-9}\ \text{m/s} \end{aligned} \tag{3.39}$$

The coefficient of consolidation can now be determined using Equation 3.40 derived by Terzaghi (Sällfors & Alén, 2012), Where the permeability of the clay and the block are as in equation (3.38) and (3.39) and the modulus calculated presented in Equation 3.33.

$$\begin{aligned} c_{v,block} &= \frac{k_{v,block} \cdot M_{block}}{\gamma_w} = 8.397 \cdot 10^{-6}\ m^2/s \\ c_{v,soil} &= \frac{k_{v,soil} \cdot M_{soil}}{\gamma_w} = 6.845 \cdot 10^{-7}\ m^2/s \end{aligned} \tag{3.40}$$

When approaching the time factor, the drainage paths for the block and soil need to be determined. For the block, the drainage path was determined to be one-sided only through the surface. The length of the drainage path was therefore decided to be the whole 20 meters. For the underlying soil, the drainage path was more double sided. This is partly due to the friction layer above the bedrock but also because drainage can occur upward through the block. Since the permeability of the blocks is significantly higher than that of the surrounding soil, the effective drainage path cannot simply be assumed to be half the layer thickness, as would be the case for ideal double-sided drainage (Swedish Deep Stabilization Research Centre et al., 2006). At the very middle of the layer the water tends to drain upwards because of the higher permeability of the block. According to the reference project an additional 2.5 m is added to the drainage path based on an engineering judgment. This drainage path is illustrated in Figure 3.10.

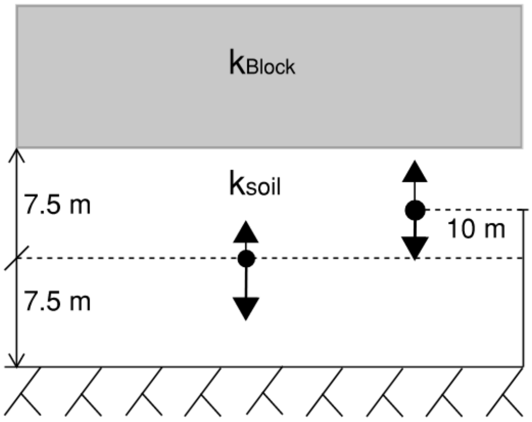

Figure 3.10: Illustration of the drainage paths for water in the underlying soil. The length of the arrows visualize the probability of the water molecule draining in either direction

The time factor of the consolidation can now be determined for both the block and the soil, see Equation 3.41.

$$\begin{aligned} T_{v,block} &= \frac{C_{v,block} \cdot t}{h^2} = \frac{8.397 \cdot 10^{-6} \cdot t}{20^2} \\ T_{v,soil} &= \frac{C_{v,soil} \cdot t}{h^2} = \frac{6.845 \cdot 10^{-6} \cdot t}{10^2} \end{aligned} \tag{3.41}$$

Using the time factor for the consolidation, it is now possible to determine the factor of consolidation, U_v, following the Equation 3.5 shown previously. The factor of consolidation is multiplied with the total settlements to determine the settlements over time, which is shown in Figure 3.11. The total settlements are also shown in Table 3.3, under "Thesis II".

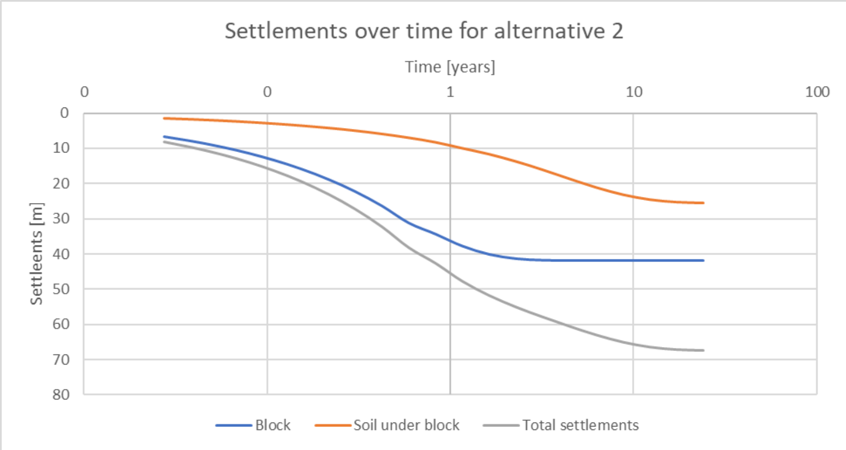

Figure 3.11: Settlements over time for the stabilized block, the soil underneath, and the total settlements

To validate the method used for the hand calculations in this thesis, the consolidation settlements calculated using alternative 1 and 2 can be compared to the consolidation settlements provided by the hand calculations in Report 15. Figure 3.12 shows the comparative consolidation settlement over time, for the stabilized block, and underlying soil and the total settlements from the report, as well as this thesis. The calculated settlements and consolidation responses align well with the report, especially alternative 2 utilizing the elastic-plastic zonation. Alternative 1 instead overestimates the settlement in the block, whilst slightly underestimating the settlement in the underlying soil.

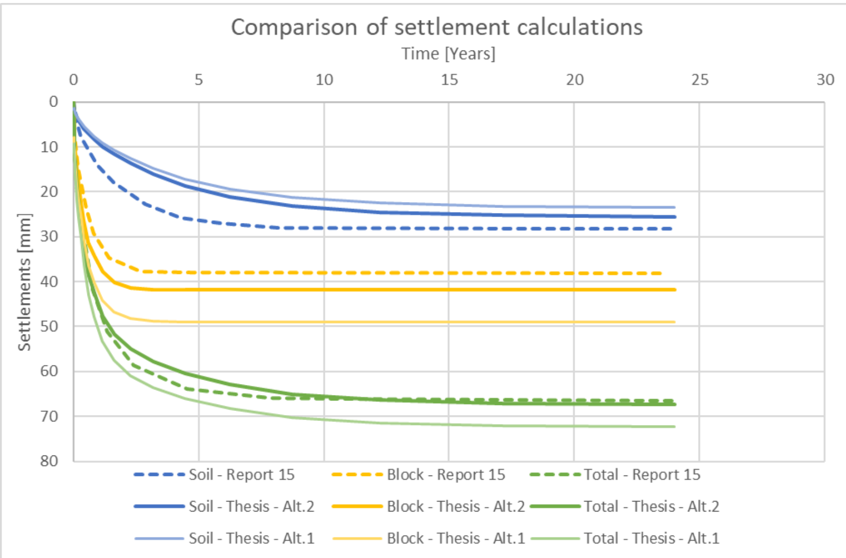

Figure 3.12: Consolidation settlements from the report, compared to the hand-calculations

3.3.1 Creep Settlements

When considering creep in addition to consolidation settlements, some additional variables are needed. The time factor from Equation 3.41 is used in addition to a specific creep-speed factor - Ψ -. The creep-speed factor is determined using the representative compression modulus, the representative creep parameter - r -, as well as the initial excess pore water pressure, represented in Equation 3.42.

$$\Psi = \frac{M}{r \cdot q} \tag{3.42}$$

The creep parameter in turn is determined as a function of depth and the incremental effective stresses, for the underlain soil, a representative value can be determined as well.

$$r(z, \Delta\sigma') = 3500 \cdot (1,3 - \frac{\sigma'_0 + \Delta\sigma'}{\sigma'_c})^3 + 200 \tag{3.43}$$

$$r_{soil} = \int_{20}^{35} \frac{r(z, \Delta\sigma'/2)}{15} dz = 483 \tag{3.44}$$

The creep calculations were made utilizing the same excel-tool that was used in the original report (Swedish Deep Stabilization Research Centre et al., 2006). The provided final settlements are shown in Table 3.4, while the full excel-sheet for the calculations can be found in Chapter B in Appendix.

Table 3.4: Consolidation, creep, and total settlements for the block and soil after 24 years

Settlements ->	Consolidation [m]	Creep [m]	Total [m]
Block	0.04	0.05	0.09
Soil	0.01	0.26	0.27
Total	0.05	0.31	0.36

3.4 Compression Strength in the Columns f_{lcc}

The compressive strength - f_{lcc} -, in the columns has two contributions. One originates from the intrinsic compressive strength of the columns themselves, while the other results from the lateral confinement provided by the surrounding soil pushing against the columns. This physically means that with increased depth, the lateral support provided by the surrounding soil increases when the in-situ soil pressure is higher, preventing the column from bulging and failing. This earth pressure theory explains why the bearing capacity of a column is not constant, but increases with depth even if the column material itself is uniform. The expression for f_{lcc} can therefore be written as shown in Equation 3.45 (Alén, 2009).

$$f_{lcc} = k_{c'} \cdot c'_{col} + k_h \cdot \sigma'_h \tag{3.45}$$

where the coefficients $k_{c'}$ and k_h are defined in Equation 3.46 and they follow the same concept as in the active and passive earth pressure theory.

$$k_{c'} = \frac{2 \cdot cos\phi'}{1 - sin\phi'}$$
$$k_h = \frac{1 + sin\phi'}{1 - sin\phi'} \tag{3.46}$$

c'_{col} is the cohesion intercept for the columns and is proportional to the undrained shear strength with an empirical relation as:

$$c'_{col} \approx (0.4 - 0.45) \cdot c_{u,col} \tag{3.47}$$

In this project the c'_{col} was already given as 75 kPa and therefore used directly.
σ'_h on the horizontal attribution of both the effective vertical in-situ stress as well as the stress increment. This is calculated through Equation 3.48 (Alén, 2009).

$$\sigma'_h = k_0 \cdot \sigma'_{v0} + 0.5 \cdot \Delta\sigma'_{soil} \tag{3.48}$$

Utilizing the equations above, the short-term failure load of the columns can be calculated by Equation 3.49. $P_{failure}$ in turn gives the maximum stress increase in the columns as $\Delta\sigma_{col} = f'_{lcc} - \sigma'_{v0}$ (Swedish Deep Stabilization Research Centre et al., 2006).

$$P_{failure} = f_{lcc} \cdot A_{col} = [\frac{2 \cdot cos\phi'}{1 - sin\phi'} \cdot c'_{col} + \frac{1 + sin\phi'}{1 - sin\phi'} \cdot \sigma'_h] \cdot \frac{\pi \cdot d^2}{4} \tag{3.49}$$

The results of $P_{failure}$ for the first 10 meters are presented in Table 3.5

Table 3.5: The short-term failure load of the columns vs. depth

z [m]	0	2	4	6	8	10
P_{failure} [kN]	81.5	93.4	99.7	106.3	113.3	120.6

4

Material Models

Materials have different mechanical behavior therefore varying constitutive models are used to capture these responses accurately. Since different materials are characterized and defined by differing behaviors and parameters, the models used in the simulations need to be well suited for the materials used in the test, and the behaviors that need to be accounted for. The available models vary in complexity in conjunction with their accuracy, as such there is a need to select a model that can simulate the desired behaviors as accurately as possible, without being too complicated or requiring parameters that are not possible to attain in this case.

In this chapter, the chosen material models will be described, partly in the methodology behind them, the behaviors they cover as well as the parameters required to use them.

4.1 S-CLAY1S

Natural soft soils have an anisotropic behavior due to their history of deposition, one-dimensional consolidation and later deformations (Wheeler et al., 2003). By taking this anisotropy into account when simulating soft soil response under loading, more accurate behaviors can be observed (Karstunen & Koskinen, n.d.). Ignoring this property in simulating the soil's response under loading can lead to inaccurate results. The constitutive model S-CLAY1S is a soil model that takes the soils anisotropy into account and therefore suitable for analyzing embankments or foundations on soft clays.

This model is based on the S-CLAY1 model, which is itself based on Modified Cam Clay (MCC) (Wheeler et al., 2003). S-CLAY1S can, as opposed to the prior models, account for the degradation of bonding so called destructuration (Karstunen, Krenn, & Vogler, 2006). The anisotropy and bonding are described by inclining the yield surface, and by an intrinsic yield surface, respectively. Figure 4.1 shows the failure surface in 3D and triaxial stress space.

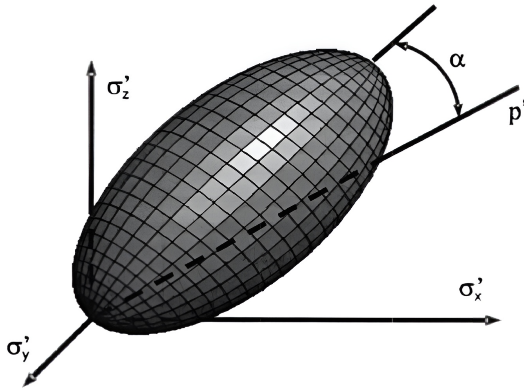

(a) 3D stress space
(Karstunen et al., 2005).

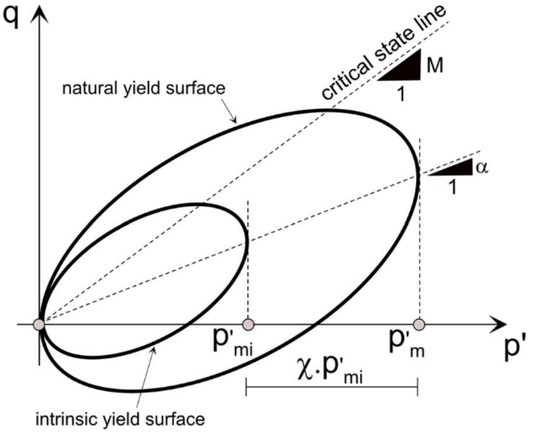

(b) Triaxial stress space
(Abed, Vogler, & Karstunen, 2026).

Figure 4.1: The yield surfaces for the S-CLAY1S model

The larger inclined yield surface Figure 4.1b represents the natural yield surface of the clay, corresponding to the unbonded state, whereas the inner surface represents the intrinsic yield surface. These are the same shape but are related in size (p'_m and p'_{mi}) via the the amount of bonding - χ - (Gens & Nova, 1993). CSL stands for the critical state line and its increment - M - critical state value of the stress ratio in triaxial space (Karstunen et al., 2005).

4.1.1 Material Parameter

To attain the model parameters for S-CLAY1S some tests such as a fall cone test, oedometertest, undrained traixial test, and finally a model calibration is needed. These tests are not complicated and therefore obtaining parameters are not considered difficult being an advantage of this material model (Abed, Vogler, & Karstunen, 2026). The material parameters required to model the soil using S-CLAY1S are summarized in Table 4.1.

Parameter	Descriptor	Unit
γ	Unit Weight	kN/m^3
κ	Swelling index	-
ν	Poisson's ratio	-
λ	Compression index	-
M	Stress ratio at the critical state in triaxial compression	-
ω	Absolute rate of rotational hardening	-
ω_d	Relative rate of rotational hardening due to deviatoric strain	-
ξ	Absolute rate of destructuration	-
ξ_d	Relative rate of destructuration due to deviatoric strain	-
POP	Pre Overburden Pressure	-
e_0	Initial void ratio	-
α_0	Initial inclination of the yield surface	-
x_0	Initial bonding parameter	-
k	Permeability	m/day

Table 4.1: List over required material parameters for S-CLAY1S Model

Beyond the parameters available in Report 15, additional ones are needed to capture the bonding and destructuration accurately. The initial inclination of the yield surface - α_0 - is as such which requires the stress path during one-dimensional consolidation - η_{K_0} - , see Equation 4.1. η_{K_0} in turn uses the critical friction angle assumed to be constant φ' , as well as the stress ratio at critical state M (Vogler, 2008). See Equation (4.2) and (4.3). In the case of Nödinge the critical friction angle was not provided and based on experience of Gothenburg clay conditions and empirical judgment the value 30° is assumed in this thesis.

$$\alpha_0 \approx \frac{\eta^2 k_0 + 3\eta k_0 - M^2}{3} \tag{4.1}$$

$$M = \frac{6 \cdot sin\varphi'_{cv}}{3 - sin\varphi'_{cv}} \tag{4.2}$$

$$\eta_{K_0} = \frac{\sin\varphi'_{cv}}{1 - \frac{2}{3}\sin\varphi'_{cv}} \tag{4.3}$$

The relative effectiveness of the rotational hardening - β - can also be determined using M and η_{K_0}, see Equation 4.4 (Vogler, 2008). The absolute effectiveness of the rotational hardening - μ - can be determined using the slope of the compression line λ, this is an empirical relationship which is validated for Scandinavian clays as presented in Equation 4.5.

$$\beta = \omega_d = \frac{3\left(4M^2 - 4\eta_{K_0}^2 - 3\eta_{K_0}\right)}{8\left(\eta_{K_0}^2 - M^2 + 2\eta_{K_0}\right)} \tag{4.4}$$

$$\mu = \omega = (10 \ldots 20)/\lambda \tag{4.5}$$

The stiffness of the clay is defined by the swelling and compression index. These parameters were obtained by the CRS-tests accessed through Skanska archives. The slope of the compression line λ and swelling line κ are determined graphically for four different depths (See Chapter A in Appendix), which were assumed to be representative of the layers defined in the simulations.

In the S-CLAY1S model, bonding and destructuration are captured by introducing the intrinsic yield surface, which represents the state where bonding between soil particles is lost (Gens & Nova, 1993). The intrinsic compression behavior can be interpreted from CRS-tests as the second slope of the compression curve, as visualized in Figure 4.2a. In the case of Nödinge, the available CRS-tests do not clearly reach the intrinsic state. This may be either due to persistent bonding within the clay particles or to insufficient compression to fully restructure the soil, see Figure 4.2b. Therefore natural compression line - λ - were determined in the initial calculation. Later all the parameters were optimized using the Soil Test function in PLAXIS to better match the relevant CRS-curves. In Tables C.1 and C.2 in Appendix, the parameters for S-CLAY1S are presented, and the values before conducting the Soil Test are also included for the sake of comparison.

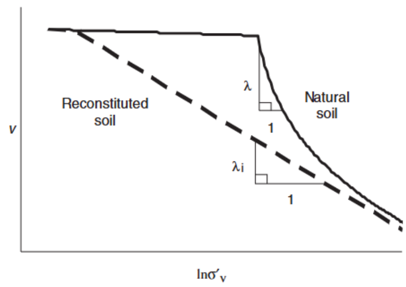

(a) Oedometer curves for natural and reconstituted soil (Karstunen et al., 2006).

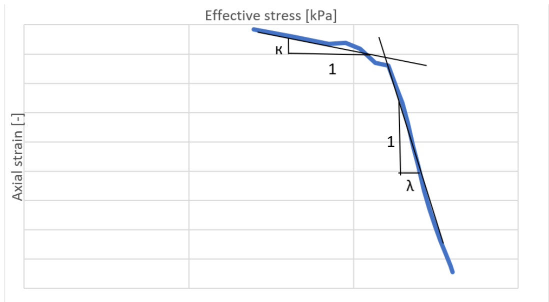

(b) CRS-test from Borehole 6607A at 21 m depth Nödinge (WSP/BohusGeo, n.d.)

Figure 4.2: Visual determination of the slope of the compression and swelling lines.

4.2 MNHard Model

The columns in VAT are modeled using MNHard material model (Benz, 2007). At the time of this thesis, the model available in the VAT model is the MNHard model, which was provided to the authors. But the reason why this model was used in VAT in the first place was due to previous studies evidencing that it provides a more realistic representation of soil behavior than the Mohr–Coulomb (MC) (Abed, Vogler, & Karstunen, 2026).

As the LCC introduce a binder into a normally or lightly over-consolidated soil, its mechanical behavior gets affected. Instead of responding primarily based on density through volumetric hardening, the treated soil begins to behave more like a coarse-grained material, where strength development is governed mainly by frictional/shear hardening (Abed, Vogler, & Karstunen, 2026). MNHard model captures this behavior and therefore used in this framework.

This model is a shear hardening elastoplastic model. In the formulation of the model the elastic share of the shear strain is considered to be small and therefore the plastic part is considered as the main. Additionally the total shear strain is assessed with no volumetric hardening (Abed, Vogler, & Karstunen, 2026). These plastic deformations develop progressively as a result of primary deviatoric loading, which gradually expands the shear yield surface toward the ultimate shear failure surface. The failure criterion defining the yield surface is reached when the mobilized friction angle reaches the maximum available internal friction angle. At this stage, the shear yield surface coincides with the Matsuoka–Nakai (MN) shear failure surface. MN-failure criteria and Mohr-Coulomb (MC) Criteria share some approaches as they predict the same shear strength under triaxial compression and extension conditions. However, the MN model predicts slightly higher shear resistance under other stress paths, such as plane stress conditions.

The failure surface for MC is considered very conservative for intermediate principal stress states between triaxial compression and extension. In addition the corners in the failure surface makes it computationally tricky (Vogler, 2008). MN on the other hand results in a smoother yield surface. As a result the model offers a relatively straightforward numerical formulation, making it attractive for practical implementation (Abed, Vogler, & Karstunen, 2026). This difference is visualized in Figure 4.3.

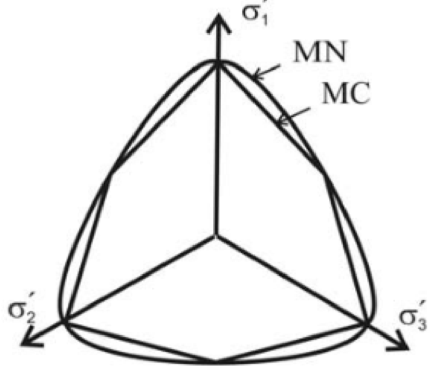

Figure 4.3: Matsuoka-Nakai (MN) and Mohr-Coulomb (MC) failure criterion in octahedral (Vogler, 2008)

A basic idea of the model in primary triaxial loading is the hyperbolic relation between strain and deviatoric stress (Vogler, 2008). During primary deviatoric loading, the soil stiffness progressively decreases as plastic strains begin to develop. The magnitude of these strains is governed by the confining stress - E_{50} -, and the unloading–reloading behavior governed through the Young's modulus - E_{ur}-.

This hyperbolic stress–strain relationship is illustrated in Figure 4.4. The ultimate deviatoric stress - q_f - is defined as $0.9 \cdot q_a$, where - q_a - represents the asymptotic value of the hyperbolic stress and the factor 0.9 is a recommended default value (Vogler, 2008).

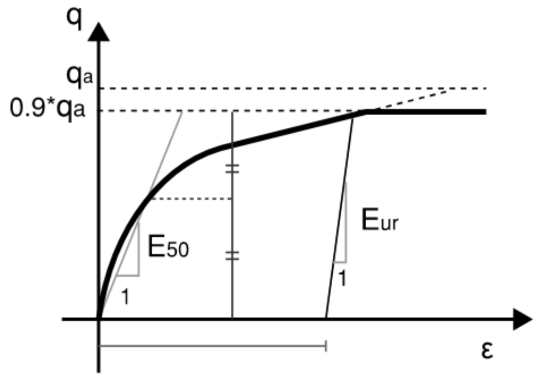

Figure 4.4: The hyperbolic stress-strain relationship

In the MNHard model, instead of E_{50}, the reference stiffness E_{50}^{ref} associated with the atmospheric pressure of 100 kPa - p'_{ref} - is used. The stiffness modulus is stress dependent and obtained as a secant modulus for mobilizing half of the maximum shear strength calculated by Equation 4.6 (Vogler, 2008). The stress dependent behavior is in contrast to the Swedish method which assumes a constant value over the whole domain and therefore needs to be considered in obtaining the material parameters.

$$E_{50} = E_{50}^{ref} \left(\frac{c' \cos\varphi' + \sigma'_3 \sin\varphi'}{c' \cos\varphi' + p'_{ref} \sin\varphi'} \right)^m \tag{4.6}$$

4.2.1 Material Parameters

Table 4.2 summaries the required material parameters for modeling columns using the MNHard model.

Parameter	Descriptor	Unit
γ	Unit Weight	kN/m^3
G_{ref}	Reference shear modulus	MPa
ν	Poisson's ratio	–
ϕ_{max}	Maximum friction angle	°
C_{ref}	Cohesion	kPa
ψ	Dilatancy angle	°
m	Power of hyperbolic stress-strain law	–
p_{ref}	Reference pressure for hyperbolic stress-strain law	kPa
R_f	Ratio of failure	–
G_{50}	Shear modulus for primary loading	MPa
k	Permeability	m/day

Table 4.2: List of required material parameters for MNHard Model

From the column properties provided in the reference project and the equations presented hereafter, the material parameters required for MNHard were calculated. The columns have a friction angle of 35° and a cohesion of 75 kpa (Swedish Deep Stabilization Research Centre et al., 2006). The Poisson's ratio is given as 0.33. Along these the young modulus of the columns E_{50} is specified as a constant value of 150 MPa. Using Equation 4.7 the reference stiffness modulus correspond to the reference stress - p'_{ref} - can be calculated. The power - m - here gives the amount of stress dependency which is chosen to be 0.7 which is considered suitable for clay (Vogler, 2008). By a similar idea, following Equation 4.8 the confining stress dependent stiffness modulus for unloading reloading is determined. These material parameters based on equations and values from Report 15 will be hereafter referenced to as "Type A".

$$E_{50}^{ref} = E_{50}\left(\frac{c'\cos\varphi' + p_{ref}\sin\varphi'}{c'\cos\varphi' + \sigma'_3\sin\varphi'}\right)^m \tag{4.7}$$

$$E_{ur}^{ref} = E_{ur}\left(\frac{c'\cos\varphi' + p_{ref}\sin\varphi'}{c'\cos\varphi' + \sigma'_3\sin\varphi'}\right)^m \tag{4.8}$$

The MNHard model in PLAXIS requires the shear modulus - G - instead of the Young's modulus directly, as part of the material definition. G can be determined using Equation (4.9) and (4.10).

$$G_{50}^{reff} = \frac{E_{50}^{ref}}{2(1+\nu-)} \tag{4.9}$$

$$G_{UR}^{reff} = \frac{E_{UR}^{ref}}{2(1+\nu')} \tag{4.10}$$

Subsequently, the parameters were optimized using Soil Test to obtain values that better represent the behavior of the columns and improve agreement with the reference triaxial response referred to as "Type B". All the parameters for MNHard including type A and B are presented in Tables C.3 and C.4 in Appendix.

4.3 Volume Averaging Technique

For the 2D simulation, a User Defined Model - UDM - in PLAXIS, so called the Volume Averaging Technique - VAT - , is employed (Karstunen, Krenn, & Vogler, 2006). VAT is a technique that allows a fully 3D problem to be represented in a 2D plane-strain, while maintaining some numerical accuracy of the simulation as well as reducing the computational costs (Becker & Karstunen, 2014).

This simplification is achieved by homogenizing the constituents of a composite material into an equivalent uniform medium while still applying independent constitutive models for the individual components, i.e. soil and column (Abed, Vogler, & Karstunen, 2026). This technique is implemented in PLAXIS 2D following the main steps provided by Abed.A where the surrounding soil is modeled using S-CLAY1S and columns modeled using MNHard model (Abed, Vogler, & Karstunen, 2026).

VAT is formulated under a set of assumptions on which the calculations are based on.This technique is based on the fundamental averaging equation where the total averaged stress rate in the composite material - $\dot{\sigma}^{eq}$ - is calculated using the total stresses for the column and soil, as well as their respective volume fractions, see Equation 4.11 (Abed, Vogler, & Karstunen, 2026).

$$\Delta\sigma^{eq} = \Omega_s \Delta\sigma^s + \Omega_c \Delta\sigma^c \tag{4.11}$$

$$\Delta\varepsilon^{eq} = \Omega_s \Delta\varepsilon^s + \Omega_c \Delta\varepsilon^c \tag{4.12}$$

$\Delta\sigma^{eq}$ stands for the averaged total state rate in the new equivalent homogenized material while σ^s and σ^c represent the total stress rates in the surrounding soil an the columns, respectively. The same concept applies to Equation 4.12 where $\Delta\varepsilon^{eq}$ stands for the rate of strain tensors. These are averaged by the parameters Ω_s and Ω_c correspond to the volume fractions of the soil and column, describing the relative share of each component in carrying the applied loads which is dependent on the geometric arrangement of the columns.

This method is only applicable with periodic distributions of the columns and assuming no slip between the soil and structure elements (Abed, Vogler, & Karstunen, 2026). By the perfect bonding both elements deform equally in the vertical direction and therefore the Kinematic constrains are met through Equation (4.13) and (4.14). Later Equation (4.15) to (4.18) fulfills the local mechanical balance through the perfect bonding considering x and z as horizontal axis and y to be the vertical axis.

$$\Delta\varepsilon_{yy}^{eq} = \Delta\varepsilon_{yy}^{c} = \Delta\varepsilon_{yy}^{s} \tag{4.13}$$
$$\Delta\gamma_{xy}^{eq} = \Delta\gamma_{xy}^{c} = \Delta\gamma_{xy}^{s} \tag{4.14}$$
$$\Delta\sigma_{xx}^{eq} = \Delta\sigma_{xx}^{c} = \Delta\sigma_{xx}^{s} \tag{4.15}$$
$$\Delta\sigma_{xy}^{eq} = \Delta\sigma_{xy}^{c} = \Delta\sigma_{xy}^{s} \tag{4.16}$$
$$\Delta\sigma_{zz}^{eq} = \Delta\sigma_{zz}^{c} = \Delta\sigma_{zz}^{s} \tag{4.17}$$
$$\Delta\sigma_{zy}^{eq} = \Delta\sigma_{zy}^{c} = \Delta\sigma_{zy}^{s} \tag{4.18}$$

Consequently from the equations above a suitable stress-strain relationship and material stiffness matrix can be developed as presented in Equation (4.19) and (4.20).

$$\Delta\mathbf{D}^{eq}\boldsymbol{\varepsilon}^{eq} = \Omega_s\mathbf{D}^s\boldsymbol{\varepsilon}^{s,eq} + \Omega_c\mathbf{D}^c\boldsymbol{\varepsilon}^{c,eq} \tag{4.19}$$
$$\mathbf{D}^{eq} = \Omega_s\mathbf{D}^s + \Omega_c\mathbf{D}^c \tag{4.20}$$

These assumptions ensure local equilibrium between the soil and the columns, as well as kinematic compatibility and the validity of the constitutive relationships (Becker & Karstunen, 2014). However these assumptions are only relevant for the Serviceability Limit State (SLS) and are not applicable when approaching failure. Therefore, to assess the Ultimate Limit State (ULS) limit equilibrium is used. This assumption also inherently limits the possibility for differential soil-column settlements to be analyzed, which is a limitation when analyzing local interaction effects between columns and surrounding soil.

Based on the described concept and the corresponding models used for the VAT, the surrounding soil was first defined using the S-CLAY1S model, followed by the definition of the columns using the MNHard model as presented earlier.

4.4 Concrete Material Model

For the 3D simulations, and alternative column model - the Concrete Model - was also evaluated and compared. The Concrete Model is a non-linear elasto-plastic material model which employs a Mohr-Coulomb yield surface for deviatoric loading, combined with a Rankine yield surface in the tensile regime with isotropic compression softening (Seequent, 2025).

In difference to the MC, Concrete Materiel Model employs time-dependent strength-stiffness behavior which reflects the aging ability as in stiffness and strength increase with hardening. In addition, strain hardening-softening in compression and tension as well as creep and shrinkage are included in the model. The creep employs a viscoelastic approach while shrinkage is referred to as the isotropic loss of volume with time and independent of the stress state. With these included the total strain is not only decomposed into elastic- and plastic strain but also considers creep strain and shrinkage strain (Seequent, 2025).

In PLAXIS, the column can be modeled using either a drained or a non-porous material definition. In the drained formulation, both stiffness and strength are defined in terms of effective stress parameters, and no excess pore pressures are generated during loading (Seequent, 2025). This representation is therefore more appropriate for capturing long-term behavior.

A non-porous material, on the other hand, treats the column as a fully solid skeleton with no capacity to store or generate pore pressures. This drainage condition is typically used as a general representation of concrete structural elements. In contrast, the drained formulation is more commonly applied to situations such as semi-permeable retaining structures or tunnel linings (Seequent, 2025). In this thesis, the columns are assumed to have a higher permeability than the surrounding soil, allowing both the generation of excess pore pressures and the possibility for water flow through the material. For this reason, the drained drainage type is considered more appropriate by the authors, as it better represents the expected hydro-mechanical behavior of the system.

However, for comparative purposes and to assess the model response under the non-porous assumption, additional simulations are also performed using the non-porous drainage type for the columns.

4.4.1 Material Parameters

The behaviors that the Concrete Model captures is dependent on varying material parameters for stiffness, strength, tension and ductility. By calibrating these parameters, a more accurate simulation of how the LCC acts during loading and straining can be achieved. These required material parameters for the concrete model are summarized in Table 4.3.

Parameter	Descriptor	Unit
γ	Unit Weight	kN/m^3
E_{28}	Young's modulus after 28 days	MPa
ν	Poisson's ratio	-
$f_{c,28}$	Uniaxial compressive strength after 28 days	kPa
f_{c0n}	Normalized initial yield strength in compression	-
f_{cfn}	Normalized failure strength in compression	-
f_{cun}	Normalized residual strength in compression	-
$G_{c,28}$	Compressive fracture energy after 28 days	kN/m
ϕ_{max}	Maximum friction angle	°
ψ	Dilatancy angle	°
γ_{fc}	Safety factor for compressive strength	-
$f_{t,28}$	Uniaxial tensile strength after 28 days	kPa
f_{tun}	Normalized residual strength in tension	-
$G_{t,28}$	Tensile fracture energy after 28 days	kN/m
γ_{ft}	Safety factor for tensile strength	-
ϵ^p_{cp}	Plastic peak strain in uniaxial compression	-
a_{duct}	Increase of ϵ^p_{cp} with confining pressure	-
k	Permeability	m/day

Table 4.3: List of required material parameters for the Concrete Model

Stiffness Parameters

The stiffness parameters for the Concrete Model are simple to calculate. The Young's modulus E_{28} for the cured concrete is initially decided to be the same as $E_{col} = 150$ MPa and Poisson's ratio is the same as before, $\nu' = 0.33$.

Strength Parameters

Strength parameters encompass several material properties. The uniaxial compressive strength of the cured concrete - $f_{c,28}$ - reflects the compressive strength after 28 days of hardening. This is initially assumed to be equal as f_{lcc} (see chapter 3.4). Consequently, in order to obtain accurate and representative values for the different LC-column lengths, the depths of 6 m and 16 m were considered representative and were therefore selected as the design values for $f_{c,28}$.

$$\begin{aligned} f_{c,28,2-12m} &= 376kPa \\ f_{c,28,12-20m} &= 515kPa \end{aligned} \tag{4.21}$$

Of the models presented so far, the Concrete Model is the most data-demanding in terms of parameter determination. Consequently, the lack of laboratory data has the greatest influence on the behavior of the Concrete Model. Several of the parameters had to be estimated based on empirical correlations and available recommendations. Some guidance and recommendations are available in the PLAXIS material manual provided by Seequent for PLAXIS 3D (Seequent, 2025). In addition there is a relevant study in which this model was applied to Bangkok clay improved with Portland cement (Than & Anantanasakul, 2023). These values were based for jet-grout columns which are assumed to be more aligned with LCC behavior compared to the recommended values by PLAXIS and therefore used in this thesis.

The normalized initially yield, failure, and residual strengths - f_{c0n}, f_{cfn}, and f_{cun}, respectively, are inspired by the values from (Than & Anantanasakul, 2023). Additional visual calibration using Soil Test were conducted and compared to the triaxial tests done at the Löftaån test site by Sadek Baker, as well as calibration to match the Type A MNHard parameters. More about the calibration with Soil Test is discussed in Section 4.5.

$$\begin{aligned} f_{c0n} &= 0.15 \\ f_{cfn} &= 1 \\ f_{cun} &= 0.9 \end{aligned} \tag{4.22}$$

These strength parameters dictate how the stress-strain relationship is simulated across the different regions of hardening, softening, and residual strength, as shown in Figure 4.5.

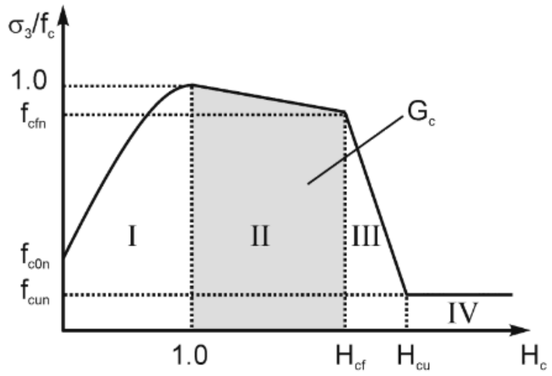

Figure 4.5: Normalized stress-strain curve in compression (Seequent, 2025).

The compressive fracture energy of the cured concrete - $G_{c,28}$ - is initially assumed to be 0,0033 kPa according to (Than & Anantanasakul, 2023), but in this thesis was calibrated through Soil Test. The friction angle ϕ_{max} is assumed to be 35° as provided which is commonly recommended value in practice. The dilancy angle was also detemind by Soil Test optimization. The safety factor - γ_{fc} - is assumed to be 1.

Just as there is uniaxial compressive strength, there is also uniaxial tensile strength - $f_{t,28}$ - which is recommended to be calculated using Equation 4.23 (Than & Anantanasakul, 2023).

$$\begin{aligned} f_{t,28,2-12} &= 0.11 \cdot f_{c,28,2-12} = 37,6kPa \\ f_{t,28,12-20} &= 0.11 \cdot f_{c,28,12-20} = 51,4kPa \end{aligned} \tag{4.23}$$

The ratio of residual vs. peak tensile strength - f_{tun} - is assumed, and recommended to be 0, while the tensile fracture energy - $G_{t,28}$ - is initially set to 0.005 (Than & Anantanasakul, 2023).

Ductility Parameters

Ductility parameters of uniaxial plastic failure strain - ϵ^p_{cp} - and the parameter controlling its increase with confining pressure - a - considerably affect the stress-strain behavior of the material. These were initially assumed to be $\epsilon^p_{cp} = -0.00246$ (Than & Anantanasakul, 2023) and $a = 16$ (Seequent, 2025), before being calibrated.

Time Dependency

The Concrete Model can simulate change in stiffness and strength due to time, i.e. time-dependent hardening. Since the columns in this case are assumed to have been hardening for 7 months before applying load, this time dependency is ignored and all stiffness and strength parameters are assumed to be the hardened values from the start.

4.5 Soil Test Calibration

To enable a one-to-one comparison between the models, it was crucial to maintain consistency in the reference data and material parameters used for the columns. To further improve the parameter basis, an additional analysis was conducted by calibrating the column parameters using the available triaxial test results from Sadek Baker (Baker, 2000). For the clay as CRS-data were already available and had been used for soil calibration therefore, it was reasonable to apply a similar approach for the columns. It should be noted that these columns were not taken from the Nödinge site specifically, but from another test site with similar soil conditions and column properties. This assumption was considered valid, as the test site is located relatively close to Nödinge.

In parallel, a reverse Soil Test calibration was performed for the Concrete Model. Since all previously presented models were based on Type A parameters, the same reference was used here, employing the previously derived MNHard parameters as input data, see Figure 4.6. The stress–strain response obtained from this simulated triaxial compression test was then used to calibrate the material parameters for the Concrete Model.

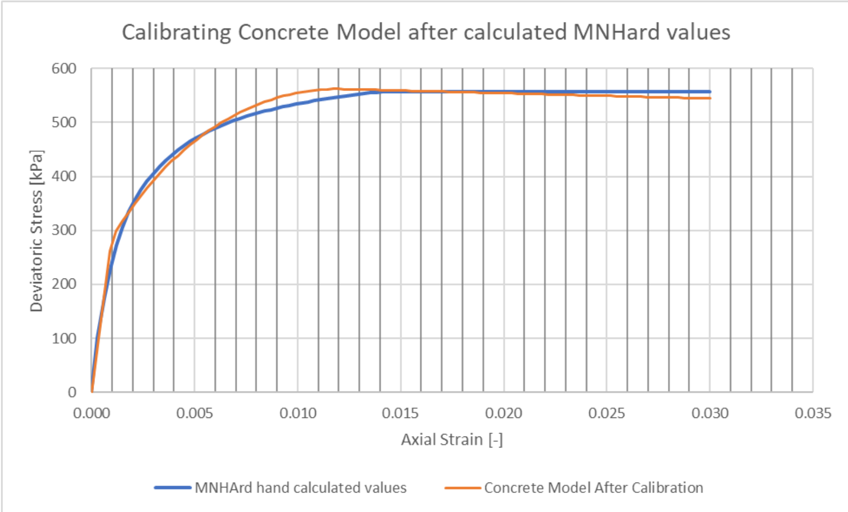

Figure 4.6: Replicating Type A MNHard parameters with the Concrete Model using Soil Test

For matching the curves the parameter optimization function in Soil Test was used and explains the large number of decimals for the parameters. It is important to note that several material parameters cannot be captured through this procedure. For example, the residual and failure strengths cannot be represented in this test, as the failure region is not reached due to the relatively small strain levels involved. Furthermore, since the MNHard model does not capture softening behavior in the same manner, these parameters remain uncertain. Therefore inspiration and initial approximation was taken from (Than & Anantanasakul, 2023), where triaxial tests on stabilized Bangkok clay was used to calibrate the Concrete Model in PLAXIS. These parameters are presented in Appendix Table C.5.

Similar as to the other models, the triaxial test provided by Sadek Baker (Baker, 2000) was used as a further improvement to obtain a more robust set of parameters to compare with the Type A parameters from Nödinge. As mentioned earlier, the test was from an area relatively close to Nödinge called Löftaån, as seen in Figure 4.7.

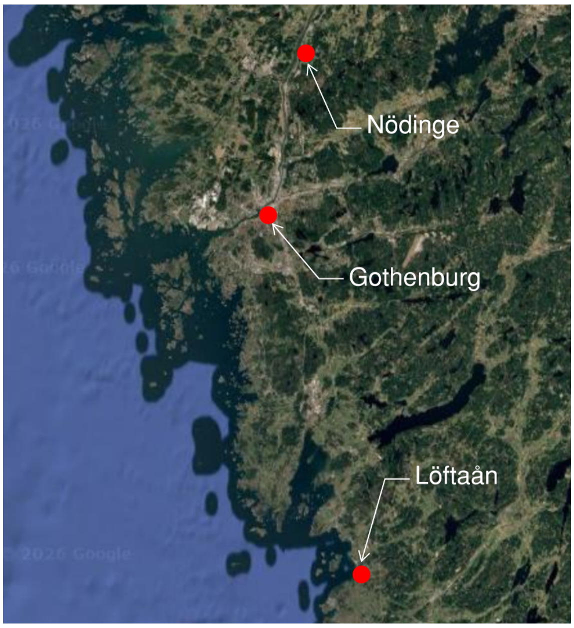

Figure 4.7: Map showing the location of Nödinge and Löftaån, in relation to Gothenburg. Modified Map from Google Maps

This test site was chosen as the most geographically and geologically similar site where triaxial laboratory data was available. It is however worth noting that these parameters will slightly vary compared to the true properties of the columns in Nödinge, and therefore the resulting settlement simulations are not a perfect representation, nor is the comparisons with the real settlement data.

The resulting deviatoric stress vs. axial strain comparison graph is shown in Figure 4.8.

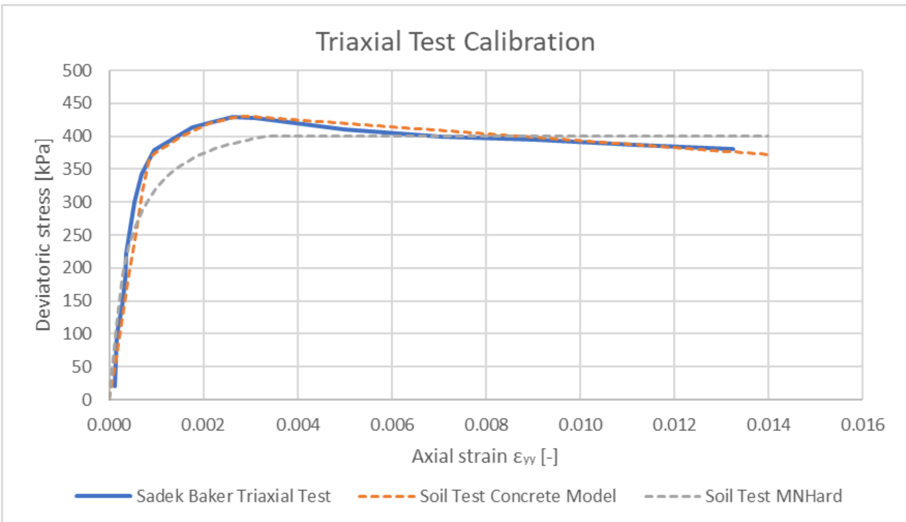

Figure 4.8: Soil Test calibration in PLAXIS for both material models, compared to real Triaxial data [Type B](Baker, 2000)

As observed in the figure, the blue line represents the reference data, while the gray line shows the calibration results after optimizing the MNHard parameters using Soil Test. Comparing the graphs produced from the Type A and Type B parameters, shown in Figure 4.9, the Type A model exhibits a less stiff response but a higher peak strength, while the optimized model shows the opposite behavior, i.e. a stiffer response but with a lower peak strength. This trend is also reflected in the comparison of parameters between Type A and Type B in Table C.3 and Table C.4.

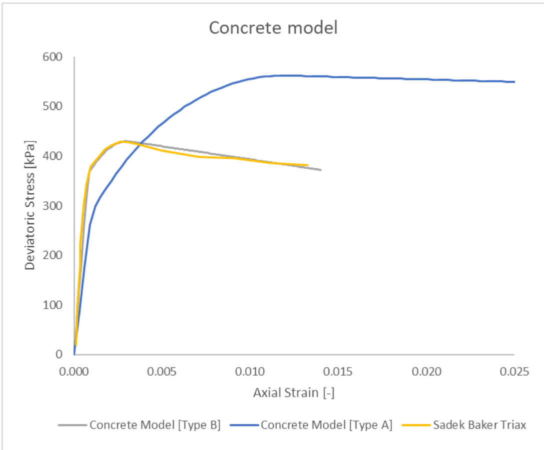

(a) The simulated triaxial tests conducted on Type A and B parameters using the Concrete Model.

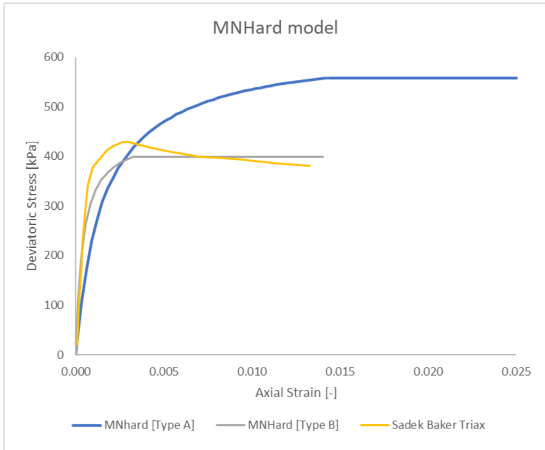

(b) The simulated triaxial tests conducted on Type A and B parameters using the MNHard model.

Figure 4.9: Simulated Triaxial tests conducted on Type A and B parameters for both material models, as well as the real triaxial data from (Baker, 2000)

The grey line on the other hand in Figure 4.9a represents the optimized Type B parameters for Concrete Model reproducing a better match, compared to the grey line in Figure 4.9b. This is due to the Concrete Model's ability to simulate both strain induced hardening and softening, as well as ductility therefore calibrating a more accurate representation for the drained LC-column behavior in compressions. The calibrated material parameters for the concrete model in this optimization are referred to as Type B and summarized in Table C.6.

5
Simulation

The first step is to use the provided data on the LC-column configuration and site characterization to apply current Swedish design practice through simplified hand calculations. Based on these results, to capture interactions that the hand calculations neglect, numerical modeling is then performed using PLAXIS in both 2D and 3D.

5.1 Geometry 2D

Due to the symmetry of the embankment only half of it is modeled as shown in Figure 5.1. For more detailed geometry setting see Chapter 2.

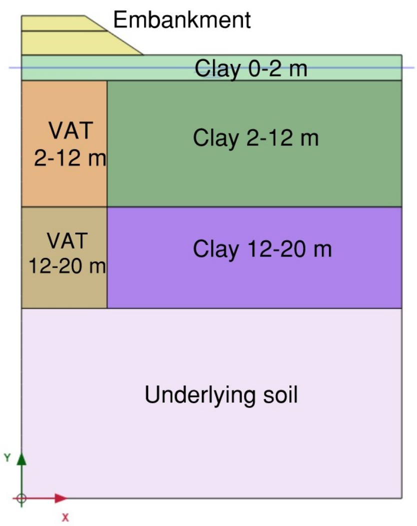

Figure 5.1: Illustration of the 2D model

The embankment is divided into two parts, as it was constructed in two phases over a period of three years. According to Report 15, the construction sequence is summarized in Table 5.1. Although these construction phases represent the real case scenario and are to be followed, some adjustments were made for the simulations. Since the columns are assumed to be installed in place, no disturbance to the surrounding soil is expected. Therefore, the consolidation phase following column installation, i.e. Phase 2 is neglected in the simulations.

According to the geological description of the project site, a thin dry crust layer is present. However, due to its limited thickness, it is neglected in the calculations, and only the properties of the underlying clay are considered. In practice, this upper layer is still reinforced, although not fully, which may lead to overly conservative simulation results if completely neglected and modeled as natural soil. Therefore, this layer is modeled as a stiffer clay with an average stiffness of 10 MPa, which is significantly higher than that of the natural clay but considerably lower than that of the designed columns.

In addition as illustrated in Figure 5.1 even if the columns start directly beneath the embankment in reality, numerical limitations made it difficult to model them in this way. On the other hand, as mentioned earlier, the upper 0.5–2 m of the columns is not fully developed due to installation limitations and therefore does not achieve the intended design strength (Swedish Deep Stabilization Research Centre et al., 2006). Based on this reasoning, the upper two meters are excluded from all results presented in Report 15 and to obtain a close comparison with the measured reference data, the same simplifications are applied in this study.

Table 5.1: The simulated construction phases following the same order as presented in report 15 (Swedish Deep Stabilization Research Centre et al., 2006)

Phase	Description	Number of days
1	Initial	-
2	Column installation	2
3	Consolidation after column installation	210
4	Construction phase 1 embankment (1.5 m)	1
5	Consolidation	660
6	Construction phase 2 embankment (total H=2.8 m)	1
7	Consolidation	379

Due to the numerical instability of the VAT model, the two consolidation stages after the two embankment construction had to be staggered for the simulation to be able to run, i.e. the 660 days of consolidation was split into 1 day, 5 day, 50 day etc.

5.2 Geometry 3D

The geometry for the 3D simulation is the same as the 2D simulation, except with a thickness of 0.75 meters, i.e. half of the centre-to-centre - c/c - distance of the columns. As such, the calculation can be done more efficiently than if the whole LC-column and the whole c/c was modeled, without losing any numerical accuracy due to symmetry on two axes. The full geometry modeled in PLAXIS 3D as well as the top down view showing the individual LC-Column can be seen in Figure 5.2.

Since the 3D simulation proved to be more numerically stable, the consolidation phases did not need to be staggered in the same way as for the 2D simulation.

The columns are still separated into 2-12 meters and 12-20 meters. This is partly due to the columns being modeled as having the same unit weight as the surrounding soil, as well as the uniaxially compressive strength being calculated as approximately 37% higher for the 12-20 meters. The other parameters are assumed to be identical, considering Soil Test was simulated to replicate only one triaxial test sample.

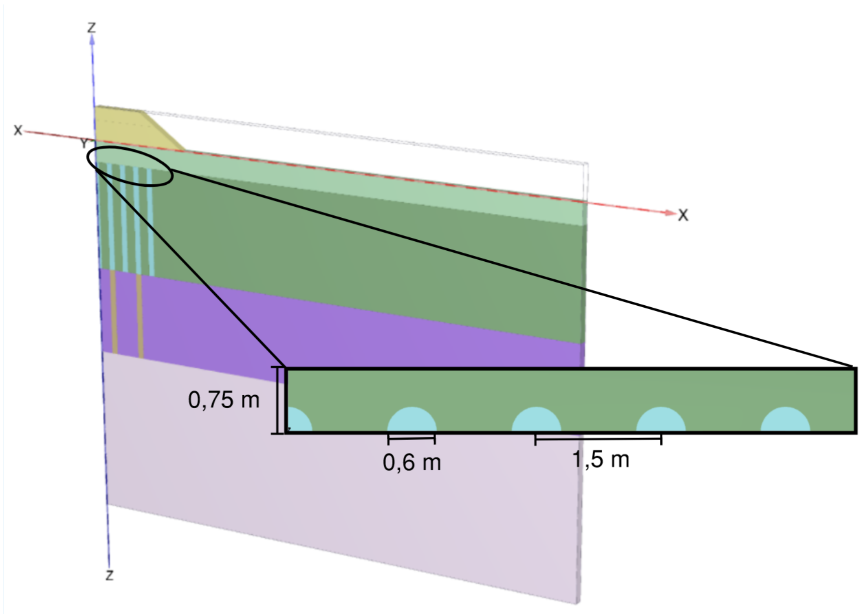

Figure 5.2: 3D geometry of the Nödinge embankment

5.2.1 Mesh Sensitivity Analysis

In a finite element analysis such as PLAXIS, the soil is discretized into a numerical mesh of nodes and elements. Since this divides a continuum into finite elements, this introduces inherent approximations in all calculations. Thus, the differential equations are not solved in a continuous form but instead over the finite number of elements and nodes. As a result of these finite elements, the computed response and results such as settlements and stresses, depend on the material models in addition to the chosen mesh density.

Therefore a mesh sensitivity analysis is performed on the three different simulations to evaluate to which extent the numerical solution is influenced by this discretization. By re-calculating the three different simulations with systematically finer mesh, the solution should approach the true response, i.e. convergence.

Plotting the total calculated settlements with the total number of nodes in the system shows a convergence after about 20 000 nodes for the Concrete Model, where the settlements remain effectively constant. The convergence is shown in Figure 5.3.

This shows that the solution has converged with respect to the density of mesh and therefore further refinement yields negligible improvements.

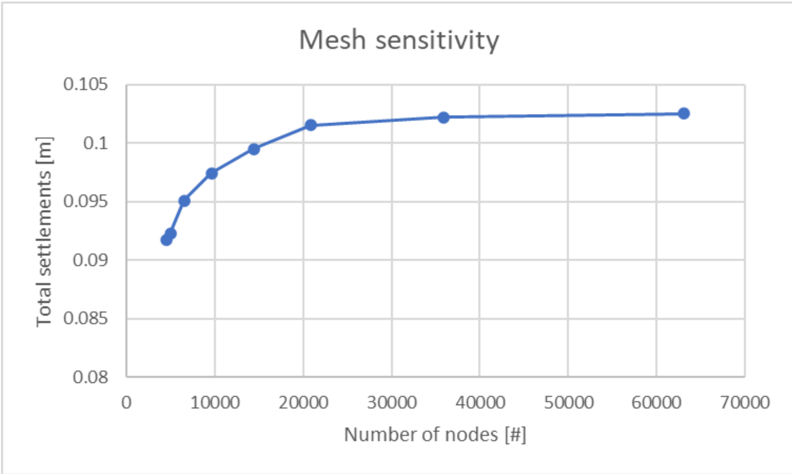

Figure 5.3: Graph showing the convergence from the mesh sensitivity analysis

The importance of analyzing mesh convergence is ensuring both numerical accuracy of the calculated settlements, as well as computational efficiency. In this case, an overly coarse mesh results in approximately 1 cm less total settlements, and such may be non-conservative in nature in addition to being less accurate. Conversely, an overly fine mesh results in computational costs and time without any real gain in accuracy. Therefore, a mesh sensitivity analysis provides a rational basis for selecting an optimal mesh with respect to both accuracy and efficiency.

5.3 Permeability Sensitivity Analysis

Since LC-columns are assumed to act as drains in some form, usually the permeability of these columns are calculated to be higher than that of the surrounding soil due to the assumption of macro-cracks developing in the LC-Columns during installation. The material in the columns itself should have lower permeability due to the dense, low-porous nature of the lime-cement mixture reacting with the soil to create a dense column. It is the formation of macro-cracks in the columns that impact the permeability to be higher than the soil. In the case of the Nödinge embankment, the permeability of the columns are assumed to be 50 times larger than the soil, and the equivalent permeability for the stabilized block is then calculated to be approximately 5 times larger (Swedish Deep Stabilization Research Centre et al., 2006). This assumption was validated from the tests conducted in the test area at Stora Viken, where it was found that the permeability was 5 to 50 times higher in these areas compared to the zones where the clay was not reinforced (Swedish Deep Stabilization Research Centre et al., 2006). Sadek Baker reveals the same relation in his study regarding the permeability of the columns versus soil (Baker, 2000).

At the time of Report 15 the LC-columns were modeled as vertical drains using LIMESET. Permeability was therefore a key parameter to capture the time dependent settlements was accurately. Even if the LC-columns are not treated in the same manner anymore a sensitivity analysis is conducted to see how the settlement response of the system is impacted with the change in column permeability. The test is conducted by initially assuming $k_{col} = k_{soil}$ and $k_{eq} = k_{soil}$, and successively increasing the column and equivalent block permeability to compare the behavior. This test is conducted on the 2D VAT analysis and the 3D analysis utilizing the MNHard model, as the Concrete Model assumed purely drained behavior for the columns, and therefore changing the permeability will not impact the simulation. The figures visualizing the settlement-over-time behavior of the simulations are shown in Figure 5.4.

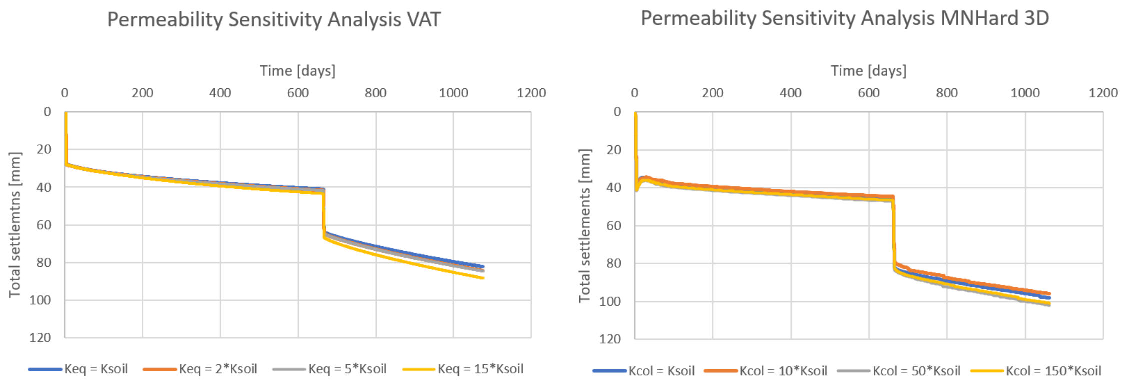

Figure 5.4: Permeability Sensitivity Analysis conducted on the VAT model (left), and the 3D MNHard model (right)

It is clear from this analysis that while the change in permeability slightly impacts the final settlements, the overall response of the system remains consistent in spite of change of permeability. As such, it is concluded that the columns' permeability are not a sensitive parameter in this case, and that the initial assumptions about column permeability can be used.

5.4 Impact of Excess Pore Water Pressure

The magnitude and dissipation rate of excess pore pressures directly influences both the immediate settlement response as well as the time-dependent consolidation behavior.

At the initial stage of loading, i.e. at the construction of the embankment, the increase of the excess pore pressure is equal to the increase of the design load since the soil behaves fully undrained initially. With time, as the soil starts to drain, the excess pore pressures start to dissipate. This dissipation of excess pore pressures are directly governed by the permeability of the soil and columns, as well as hydraulic boundary conditions.

The absolute rate of pore pressure dissipation results in the rate of consolidation. With faster dissipation comes faster consolidation. Therefore, comparing excess pore pressures provided as real measurements with simulated excess pore pressures can highlight if the design loads and the dissipation are modeled accurately or not.

For the comparison, the piezo-meter data available from the report are obtained at a depth of 14 meters, located in the center of the embankment. Two data sets of pore pressures from this depth is available, both inside a LC-Column, as well as in the soil between the columns. As the LC-Columns are the most interesting place to study the dissipation, the simulated pore pressures are extracted from PLAXIS at a depth of 14 meters, inside a column for the 3D case, and inside the block for the VAT case. The Concrete Model simulations will be excluded from this analysis, due to its specific drainage formulation ignoring pore pressure generation.

As the simulations assume that the LC-columns are "wished-in-place", there will be no excess pore pressures generated due to installation effects. As compared to the measured pore pressures, which will show generation of pore pressures during the installation of the columns.

5.5 Problems Encountered During Simulations

While PLAXIS is a robust and functioning finite element analysis program, challenges can arise when dealing with complex numerical simulations. Several errors and issues were encountered during both 2D and 3D analyses, which had to be resolved in order to successfully complete the simulations.

5.5.1 Problems in 2D

During the several different 2D VAT simulations that were made, one persistent problem was encountered many times. Several calculation phases failed multiple times with the same error: Run-time error in kernel. This vague error message was hard to deduce any information from, but some changes were found to mostly deal with this issue. Most of the time the error could be solved by simply decreasing the max load fraction for the failed calculation phase. In PLAXIS, the load fraction factor controls how much of the total load is applied in each calculation step. A load fraction of 1.0 means that the full load is applied in a single step, whereas the default value of 0.5 applies the load in two increments. Since PLAXIS uses an incremental–iterative method, with too large increments it becomes difficult to find convergence.

Using the standard value for this parameter as 0.5 resulted in failure in convergence therefore it was reduced by several magnitudes in some phases. Reducing the load fraction factor, in combination with increasing the maximum number of steps and iterations per phase, generally led to longer but ultimately successful calculations. These adjustments allow the model to stabilize numerically before progressing to subsequent increments. Since VAT combines two advanced non-linear material models, the system is more sensitive to numerical settings and therefore important to understand the calculation method PLAXIS relies on.

5.5.2 Problems in 3D

For the 3D simulations, the issues encountered were only for the MNHard simulation. The solver types available in PLAXIS 3D are the following: Classic (Single-core iterative), Paradiso (Multicore direct), and Picos (Multicore iterative). These vary in robustness, speed and efficiency, therefore, an error in Picos solver can usually be solved by changing the solver type to Paradiso or Classic which increases the robustness at the cost of speed. During several simulations, error messages from all of these solvers were encountered, usually "incorrect solution, slow convergence" or "error in iterative solver". Another error encountered was that of "Stiffness matrix is nearly singular and cannot be solved", this usually happened due to poor mesh quality. When generating a mesh in 3D, most times some warnings were displayed about mesh errors that could only be bypassed by increasing the mesh quality to more than what was decided neccessary due to the mesh sensitivity analysis. The error appeared not only when the mesh was too poor/coarse, but also when the mesh was overly fine.

6
Results

This chapter presents the results of both 2D and 3D simulations performed in PLAXIS. In the 3D simulations the results include cases based on the initial parameters from the reference project i.e. Type A, as well as updated parameters derived from Soil Test data i.e Type B which are later compared.

6.1 Settlements

As presented in Chapter 3 using traditional Swedish design methods and simplified hand calculations resulted in a Green Field total settlement of 1.74 m, with full consolidation occurring over a period of approximately 160 years. After reinforcement with LC-columns, the settlements were reduced to approximately 0.06–0.07 m after 20 years and excluding creep. For better comparison see Table 3.3.

The calculated values are consistent with those presented in the reference project as well as with the available measured data, see figure 6.1. The next step is then to reproduce this behavior using numerical modeling, which is presented in the following sections.

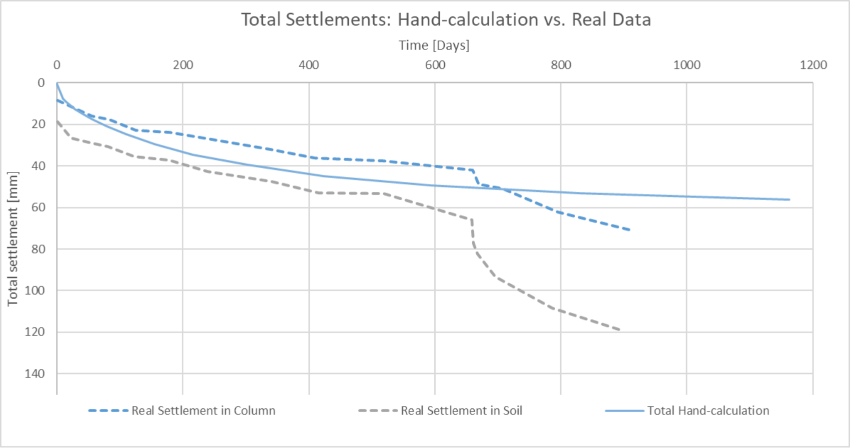

Figure 6.1: The hand calculated settlement compared to the real settlement data

6.2 VAT Validation

As observed in Figure 6.2, VAT successfully captures the overall behavior of the system. During the loading stages where the embankment is constructed, a clear immediate settlement is observed, while the consolidation behavior between the loading phases is also well captured. The settlement response lies in between the real settlement for soil and the columns.

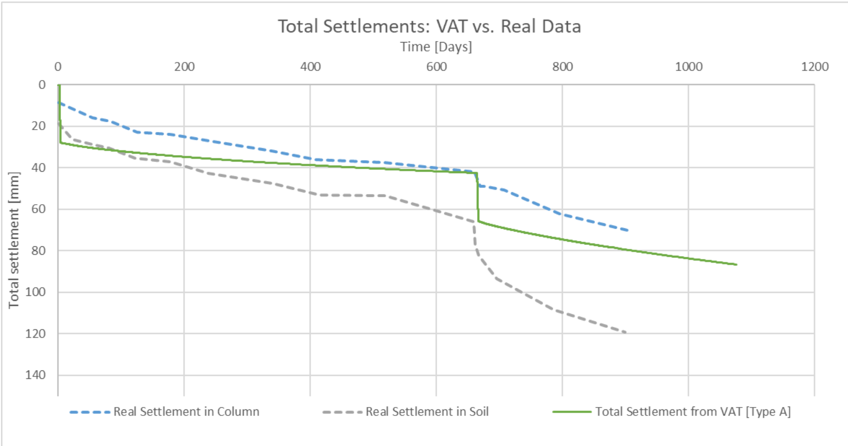

Figure 6.2: The simulated settlements using VAT, compared to the real settlement data

Figure 6.3 shows the simulated settlements validated against field measurements obtained from bellow hoses in the middle of the embankment, from both inside a long column, as well as the soil between columns. As observed in the early few meters the VAT settlements lie between the columns and the soil which reflects the results in Figure 6.2. However, further down, the VAT simulation underestimates the settlement for the block, while overestimating the settlement for the underlying soil.

As the measurements show the first 7 meters the soil settles much more than the columns, which reflect the effect of the soil hanging on the columns and the catenary arching effect from the load distribution. After that they both exhibit very similar settlements indicating a strong interaction and near perfect contact between them. Since this response is observed in most part of the stabilized block the assumption behind both the Swedish Method and the VAT regarding perfect bonding is strengthened and once again proves plane sections remain plane.

The presented bellow hose inside the long column only includes measurements reaching 18 meters deep into the ground (Swedish Deep Stabilization Research Centre et al., 2006). Although no measurements are available below that, it is expected to see indications of the column punching into the clay at around 20 meters depth.

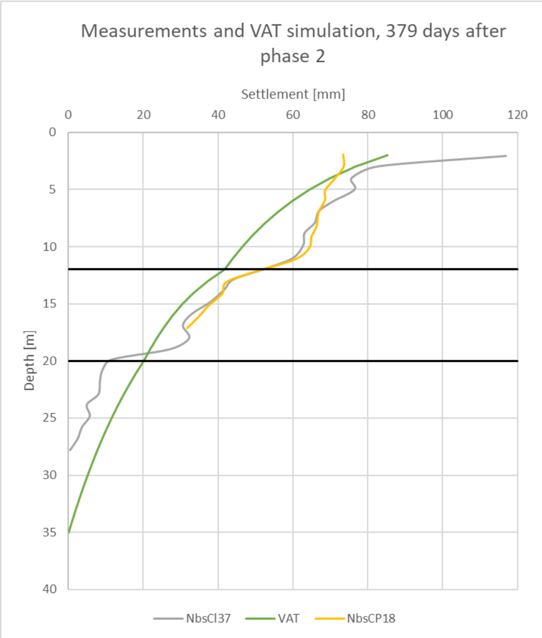

Figure 6.3: Settlements versus depth measured inside an LC column (NbsCp18) and in the surrounding soil (NbsCl37) (Swedish Deep Stabilization Research Centre et al., 2006), compared with VAT simulations 379 days after final construction

In addition to the bellow hose measurements mentioned above, additional settlement-versus-depth data at different time steps during the consolidation phase after construction stage 1 were available and used to assess the VAT results. These are presented in Figure 6.4.

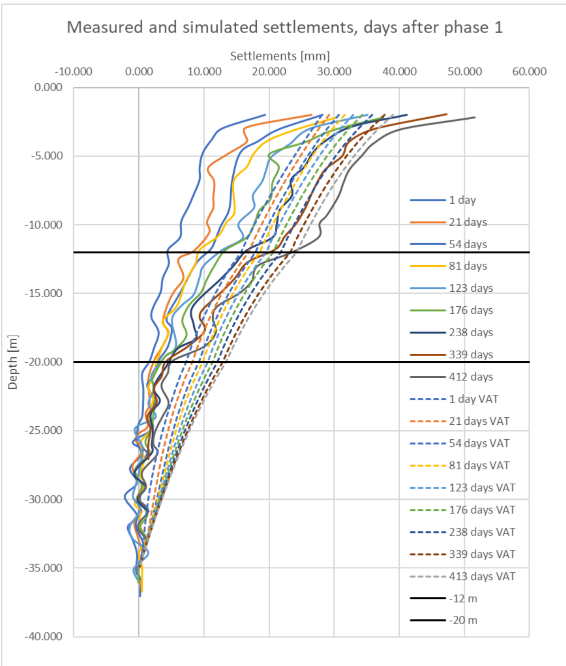

Figure 6.4: The settlement of the soil between the columns, for every depth at multiple points in time, compared with the VAT simulation

VAT does not capture the clear transitions between the stabilized block and non-stabilized soil, shows higher initial settlements, and a weaker time-dependent development. This is observed by the overestimation of the block's stiffness and the consolidation that develops more slowly and in a more linear manner in the simulation compared to the measurements. In addition in the underlying soil from 20 meters down the simulation underestimates the stiffness of the subsoil.

6.3 3D MNHard Validation [Type A]

Figure 6.5 shows the 3D simulation results using MNHard for the columns and S-CLAY1S for the soil. Similar to the VAT, the overall response is captured, and the results fall within the range of the measured data.

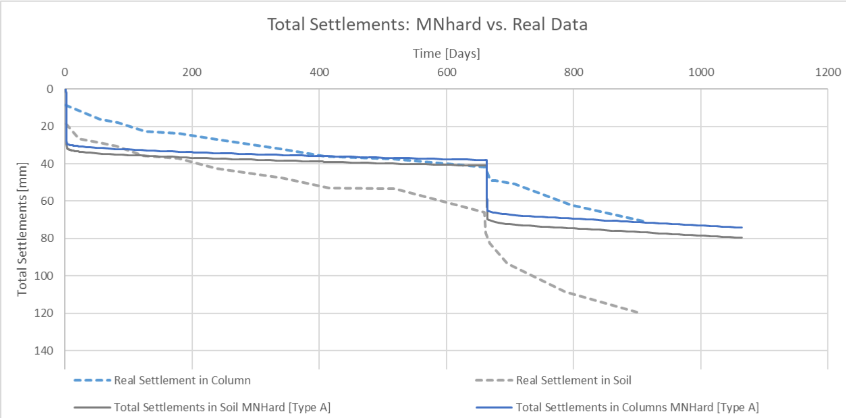

Figure 6.5: The simulated settlements using MNHard model in 3D [Type A], compared to real settlement data

The difference between the blue and grey line, which represent the settlements of the columns and soil respectively, corresponds to the differential settlements. These reach up to a maximum of 1 cm in this case after the second consolidation. In most numerical models, including the VAT approach, a key assumption is that columns and surrounding soil settle either equally or with only minor differential settlement.

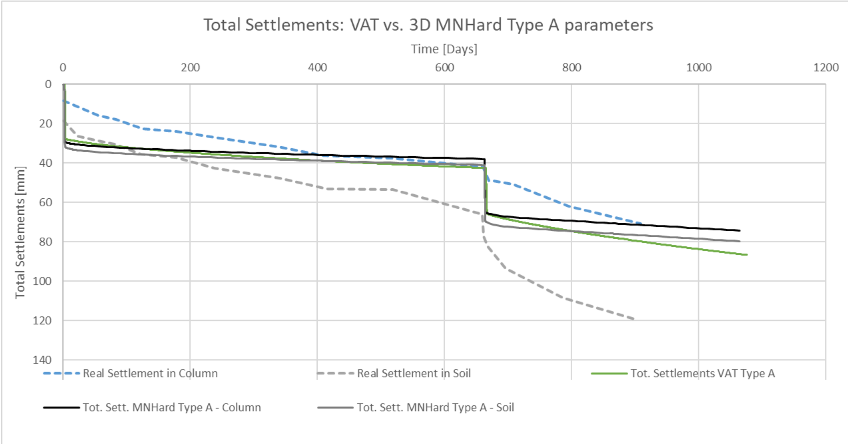

Figure 6.6: The simulated settlements using VAT and MNHard in 3D [Type A]

Comparing the VAT and MNHard 3D settlements shown in Figure 6.6, it is noticeable that the VAT simulation captures a slightly smaller initial settlement and a more pronounced consolidation settlement, especially in the later consolidation phase, while the 3D simulation shows almost no consolidation settlement and is mostly dominated by immediate settlements. It is worth mentioning that these results are only from a depth of 2 m below the embankment. To capture a better comparison in between the 2D and 3D plane the results are plotted versus depth and presented in Figure 6.7.

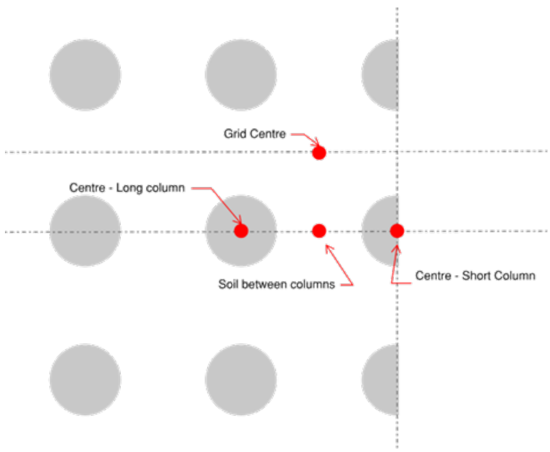

(a) Overview of the points chosen for the 3D settlement analysis.

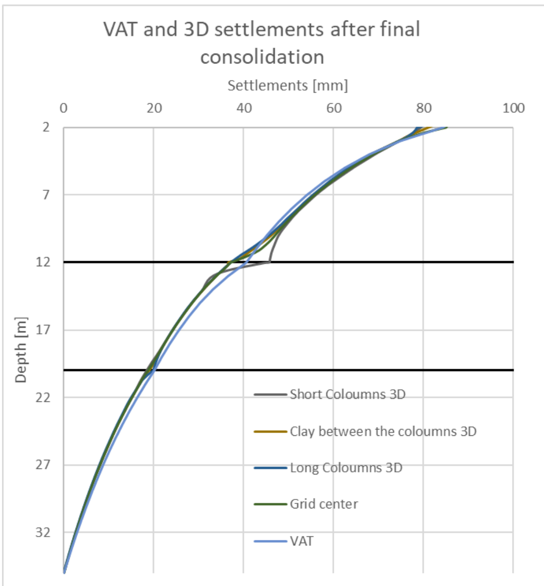

(b) Settlement over depth comparison between 3D analysis and VAT.

Figure 6.7: Settlement over depth from 3D analysis and VAT, showing close agreement between the two simulations

For this comparison, four distinct points in the 3D model, as shown in Figure 6.7, were selected and show overall good agreement. The VAT model follows the same trends observed in the long columns and at the grid center. The deviation observed for the short column at 12 m depth, where only long columns are present thereafter, is attributed to changes in load distribution and arching effects associated with the varying column lenghts, and the transition zone that happens when the load transfers from the bottom of the short column. A similar behavior is also observed in the upper 2–3 m, where the VAT model does not fully capture the transition zone and the associated arching effects between columns. Therefore some variations are observed there as well.

6.4 Concrete Model Validation [Type A]

Figure 6.8 presents the simulation results for the Concrete Model using Type A material parameters in the 3D analysis. The two avaliable drainage formulations are considered for the columns: drained and non-porous, since the undrained fomrulation is not avaliable.

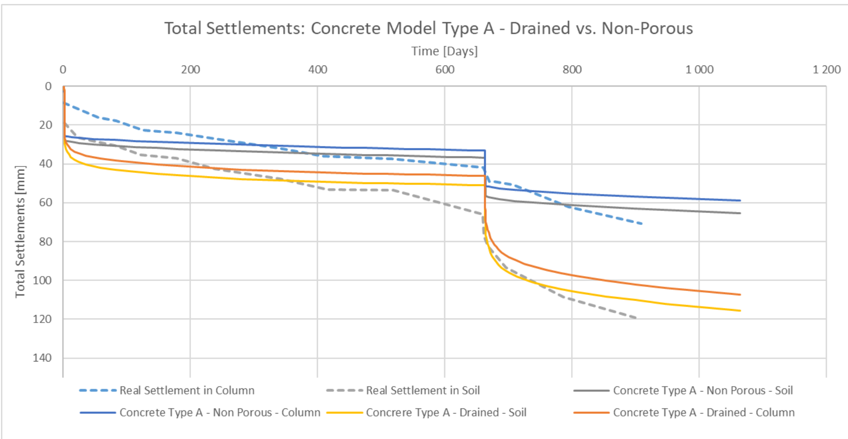

Figure 6.8: The simulated settlements using Concrete Model in 3D [Type A], utilizing both available drainage formulations, compared to real settlement data

For the drained formulation, the settlement response is characterized by large immediate settlements followed by a gradual consolidation phase. During the first construction and consolidation phases, the simulated settlements show reasonable agreement, albeit more aligned with the soil settlement compared to the column settlement overall. Following the second settlement, the difference increases, fully establishing that the simulated settlements more allign with the soil and not the column settlements that were measured, leading to overly conservative results. This pronounced settlement response is likely related to the fully drained assumption, which allows for such rapid deformations.

The non-porous formulation produces a much different response- Both the total settlement mangitude and the rate of consolidation are reduced compared to the drained formulation. The settlements remain below the lowest measured values of the columns throughout most of the simulation period, indicating an overall more stiff response of the stabilized soil.

The comparison between the drainage formulation for the Concrete Model shows the significant influence that the assumed formulation has on predicted settlement behavior. Neither of these formulations provided settlement behaviors that closely aligned with the measured values, either being overly conservative, or indicating much less settlements than measured. This demonstrates that the hydrological assumptions adopted for the LC-columns has a substantial impact on the development of settlement.

6.5 Comparison of Constitutive Models

To isolate the influence of constitutive model formulations, additional simulations were performed utilizing the Type B parameter set. These parameters were derived for the same triaxial calibration procedure and are not intended to reproduce the Nödinge field measurements. Instead they were meant to enable a more direct comparison between the MNHard and Concrete models under equivalent material conditions.

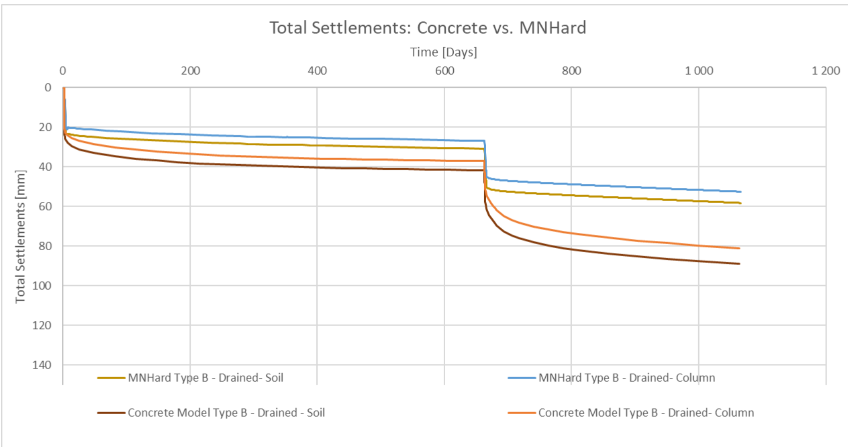

Figure 6.9: Comparison of the Concrete and MNHard constitutive models utilizing Type B parameters and the drained formulation

Figure 6.9 compares the settlement response obtained using both MNHard and Concrete models using the Type B parameter set and the drained formulation. Despite being calibrated against the same laboratory data, noticeable differences are observed between the responses. The Concrete Model predicts larger settlements throughout the simulation period and exhibits a more gradual and pronounced consolidation response compare to the MNHard model. The results indicate that the choice of constitutive model formulation alone can significantly impact the magnitude and development of settlement. Even when the parameters should be equally stiff.

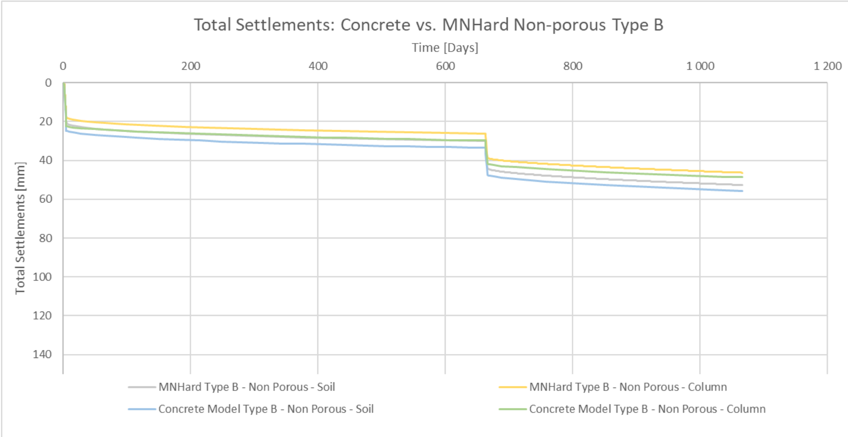

Figure 6.10: Comparison of the Concrete and MNHard constitutive models utilizing Type B parameters and the non-porous formulation

To further isolate the influence of the constitutive formulation, the same comparison was once again done, but using the non-porous drainage formulation for both models. As shown in Figure 6.10, the settlement responses become considerably more similar in this case compared to the drained case. Both models predict stiff behavior with comparable settlement magnitudes and responses. The Concrete Model still produces slightly larger settlements, but the difference is reduced compared to the drained simulations. This suggests that a significant portion of the discrepancy observed in Figure 6.9 originates in the constitutive formulation and not in the drainage formulation itself.

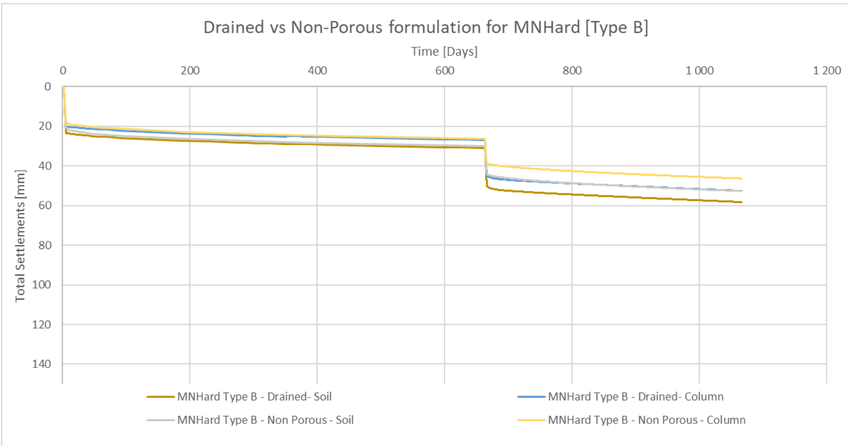

Figure 6.11: Comparing the impact of the drainage formulation for the MNHard model

To assess the influence of the drainage formulation specifically within the MNHard model, Figure 6.11 shows the non-porous and drained simulations conducted using the MNHard model. The resulting settlements are similar, with only minor differences in final settlement. These results indicate that for this case, the MNHard model is relatively insensitive to the selected drainage formulation, that being for the conditions considered in the study. This suggests that the constitutive response itself governs the predicted behavior more than the hydraulic assumptions and drainage formulations.

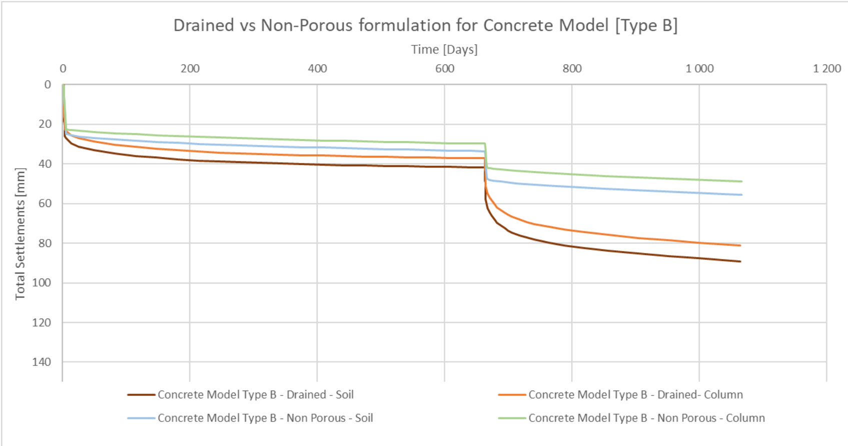

Figure 6.12: Comparing the impact of the drainage formulation for the Concrete Model

The same corresponding comparison for the Concrete Model is presented in Figure 6.12. In contrast to the MNHard model, the drainage formulation has a distinct impact and influence of the response. The drained simulation produces larger settlements and a smoother transition between the immediate settlement and the subsequent consolidation. The non-porous simulation instead exhibits a more distinct and angular settlement response, closely resembling the response from MNHard. The difference in magnitude and general behavior is much more compared to the MNHard model.

Taken together, Figure 6.9-6.12 demonstrate that the sensitivity to drainage assumption differs substantially between the models. The MNHard produces similar responses regardless of drainage formulation while the Concrete Model shows a stronger dependency on the selected formulation.

6.6 Excess Pore Water Pressure

In the reference project, excess pore pressures - u_e - were measured inside a column at a depth of 14 meters, located at the center of the embankment (Swedish Deep Stabilization Research Centre et al., 2006). These field measurements showed peak excess pore pressures of approximately 26 kPa following the first construction phase, and 20 kPa after the second phase. Approximately 15 kPa of excess pore pressure dissipated during the intermediate consolidation stage of around 660 days.

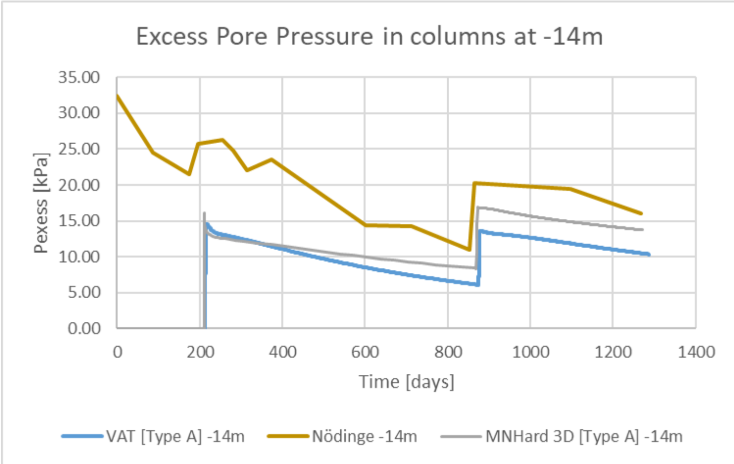

Figure 6.13: Excess Pore Pressures over time in column at 14 meters depth

As shown in Figure 6.13, the field measurements began at an initial value of 35 kPa prior to the first loading stage, assumed to be as a result of the column installation. In the numerical simulations, all models begin at 0 kPa due to the "wished-in-place" assumption.

Regarding the dissipation rates, both the VAT and MNHard 3D simulations captured the second consolidation phase with high correlation to the data, i.e. the rate of dissipation seem to be almost identical. During the first consolidation phase, the MNHard 3D simulation exhibited slower dissipation rate compared to both the VAT model and the field measurements. Both simulations underestimated the peak pore pressures by approximately 5 kPa compared to the field data. No pore pressure data was extracted for the Concrete Model within the columns.

7 Discussion

The obtained results, while straightforward especially when compared to a reference measurement, still provide several aspects worth discussing, which are addressed in this chapter.

7.1 Reliability of Material Parameters

In both the VAT and the MNHard 3D simulations, a somewhat flatter consolidation response than in the measured data was observed. There is uncertainty associated with the input parameters for both the columns and the clay, and the slower consolidation behavior may be attributed to this. The consolidation coefficient governing the rate of consolidation depends on both the stiffness (modulus) of the components and their permeability, as also mentioned in Equation 3.40. For the permeability of the columns a sensitivity analysis was conducted as presented in Section 5.3. The analysis revealed that it had negligible influence on the settlements. For the clay on the other hand, the permeability values from the reference report were used and considered reliable, and were therefore not investigated further.

The remaining key parameter is the modulus M, which was based on available CRS tests. As this was the only laboratory data available, no separate uncertainty analysis of these tests was carried out either. But looking at the results presented in Figure 6.4 the VAT simulations predict larger settlements in the underlying soil than those observed in the field. Since this layer is modeled only with S-CLAY1S, the response is controlled entirely by the clay parameters. This suggests that the adopted modulus values may underestimate the true stiffness of the soil.

A similar reasoning can be applied to the column stiffness. MNHard captures a stress-dependent stiffness, whereas the input data from the reference project of this thesis, based on the Swedish method, assumes a constant stiffness along the column depth. Even though this was intended to be accounted for, it still introduces uncertainties regarding whether the columns are modeled too conservatively or non-conservatively, which affects the consolidation response and may contribute to deviations from the reference data.

7.2 Concrete Model

For the Concrete Model, several parameters, particularly those governing softening, ductility, and fracture energy, had to be estimated from empirical correlation and a study of stabilized Bangkok clay with Portland cement. While this provided initial values, the applicability for LC-columns in Swedish soft clay is not guaranteed. Given that the strain levels reached in the simulations did not mobilize the post-peak parameters, and that the parameters mostly governing the initial stiffness response were calibrated, this poses an uncertainty as well.

The drainage type also plays a crucial role for this model. The drained Concrete Model and MNHard simulations both showed that treating the columns as fully drained increases the immediate settlement somewhat relative to the undrained case. The non-porous Concrete Model produced results most similar to the MNHard undrained case in settlement over time, though it still underestimated total settlements. This hierarchy of drainage behavior has direct implications for model selection in practice. Since consolidation behavior is of primary interest, undrained column modeling with subsequent consolidation analysis is essential, and the Concrete Model's current limitations in this regard should be clearly recognized.

As observed by the results presented in Section 4.5, the model reproduced the real triaxial test data of the LC-columns relatively well. This is mainly due to its comprehensive formulation and its ability to capture several different behaviors as in time-dependent hardening, the hardening-softening stress-strain curve, tensile failure and more. Therefore the Concrete Model shows strong potential for further use in modeling the columns for ULS analyses.

However, in this thesis, its application for SLS analyses did not demonstrate the same potential. One aspect affecting this, and worth noting, is that the maximum axial strain reached in the simulations (approximately 0.7–0.8%) places the material response firmly within the first linear softening region of the Concrete Model's stress–strain curve, between the maximum and failure strength. Parameters governing the softening, residual, and failure regions were therefore largely inactive during the simulations. This means that several of the model's most distinctive features were not mobilized in this application, and that the initial stiffness and maximum compressive strength, rather than failure-, residual strength or post-peak behavior, governed the response throughout the analyses.

There are, however, possible approaches for adjustment. In Report 15 (Swedish Deep Stabilization Research Centre et al., 2006), where LIMESET was used for modeling the columns as vertical drains, a fictive permeability was introduced, which corrected the model and thereby resulted in accurate total settlements. A similar approach could alternatively be tested using the drained Concrete Model.

Another crucial disadvantage to the Concrete Model is the lack of stress-dependent stiffness, which is in contrast to the MNHard model. The deeper into the soil that the

LC-columns are, the more lateral stress is applied to the perimeter of the columns, this pressure keeps the columns intact, thus allowing for higher stiffness. This real behaviour that LC-columns are exposed to is a crucial part of the MNHard models' formulation. Since the triaxial compression test that was used as a reference for the Type B parameters was conducted with a confinement pressure of just 20 kPa, this means that initially, at a very shallow depth, both models simulate the same stiffness. However, with increased depth and therefore increased lateral stress, the MNHard can more accurately model the increased stiffness of the columns, while the Concrete Model simulates a stiffness that is independent of depth. This leads to lower overall stiffness, and higher settlements.

This could also explain why the drainage formulation has differing impacts on the settlements when comparing the two models. For the Concrete model, the drained formulation allows the columns to behave as porous material, leading to development of effective stress distribution and volumetric compression, whereas the non-porous formulation removes the hydro-mechanical coupling within the columns letting them instead behave as solid inclusions. This affects the settlement response more than the MNHard model, where the stiffness evolution is already controlled by the constitutive model itself, leading to a smaller influence gained from the drainage formulations.

In order to further assess whether the proposed model is conservative or realistic as was one of the aims of this thesis, field measurements are required to provide a robust basis for evaluating its accuracy. In the comparison conducted in this thesis, such data were not available. Initially, the selected reference case, Nödinge, was considered to contain all the parameters required for this investigation. However, as the work progressed, it became evident that the available column properties were insufficient for analyzing a comprehensive model such as the concrete Model.

The triaxial test data that were ultimately used made the simulations possible, but these tests were primarily intended to investigate the behavior of LC-columns through large-scale laboratory experiments therefore no settlement measurements were available. As a result, the model could not be validated against full-scale field observations.

7.3 VAT vs 3D Modeling

As mentioned earlier, the proposed VAT is a simplification of a 3D problem into a 2D plane-strain model, while still maintaining comparable accuracy (Becker & Karstunen, 2014). The results obtained in this thesis also support this claim, as presented in Figure 6.7. The smaller variations observed at the surface and at 12 m depth, where the short columns end, are related to arching effects caused by the load distribution. The minor variation observed in Figure 6.6 is due to the extracted point at 2 m depth still being influenced by these arching effects.

7.3.1 Comparison of the Constitutive Models

When comparing the models used for the columns, some differences in their theoretical formulations affect the results. MNHard model's stress-dependent stiffness formulation results in higher effective stiffness at greater confining pressures, which may lead to a stiffer response in the deeper clay layers compared to what the Concrete Model's formation produces. The Concrete Model appears to develop its stiffness more gradually as loading progresses, whereas the MNHard model tends to lock in a higher stiffness at depth earlier in the loading process.

It is also worth noting that in order to have a fair one to one comparison in between the models, it is essential to keep consistently with calibrated parameters. In the case of this thesis the material parameters used were sourced from two distinct datasets, designated Type A and Type B. Type A parameters were derived from the reference project with the base column properties for the Nödinge site. Type B parameters however were obtained through Soil Test calibration against triaxial test data (Baker, 2000) of columns at the relatively nearby Löftaån test site. While the two sites are geologically similar and in relatively close proximity, the resulting parameters sets exhibit notable differences, particularly in column stiffness and cohesion. The Type B columns proved stiffer and stronger than those implied by the Nödinge data, which led to a systematic underestimation of settlements in the numerical simulations.

7.4 Pore Pressure Behavior

A persistent offset between the simulated and measured pore pressures is the starting condition. Field measurement show that excess pore pressures were already at approximately 35 kPa from the column installation and as a result of the soil disturbance and machinery weight during installation. Since all simulations used a wished-in-place approach, no installation-induced pore pressures were generated, and all models began with an excess pore pressure of 0 kPa. This means that the initial condition of the clay at the start of embankment loading was softer and more pressurized in reality than in the models, which could explain why the simulated peak excess pore pressures during loading were lower than the field measurements.

Beyond the initial offset, the dissipation rates showed generally good correspondence, especially during the second consolidation phase where both VAT and 3D MNHard matched the field data closely. The VAT performed somewhat better during the first consolidation phase, suggesting that its equivalent permeability formulation may more effectively represent the radial drainage contribution of the columns compared to the 3D model.

7.5 Creep

The absence of creep in the simulations is another simplification worth noting. In reality, creep plays a crucial role and accounts for a significant portion of the total settlements, especially having a thick layer of clay underneath the floating columns as in this case. However, in this thesis, creep was neglected due to simplifications and the complex traditional methods required to include creeps attribution. On the other hand the monitored settlement data covers only approximately three years, within which creep effects had not fully developed. However, the reference project's design target of 0.35 m total settlement after 20 years was set with creep included. For longer term assessment, neglecting creep would lead to a non conservative underestimation of total settlements, particularly in the underlying soil below the stabilized block. However, since the column configuration itself is not the focus of this study, no further evaluation of the implications of neglecting creep has been carried out.

7.5.1 Differential Settlements

The measured differential settlement of approximately 50 mm between the columns and the surrounding soil at the Nödinge embankment is notably large and exceeds what the numerical models could reproduce. The VAT inherently suppresses differential behavior through its kinematic constraint, and even the 3D simulations produced differential settlements of at most 10 mm. This discrepancy may partly reflect the influence of installations effects and the transition zone behavior at shallow depths, which are not captured in either model due to the wished-in-place assumption and the exclusion of the upper 2 m. It was also shown that the measured differential settlements occur very close to the top of the stabilized block, in a zone that is difficult to represent accurately with either modeling approach.

7.6 Numerical Stability and Modeling Limitations

Several numerical challenges were encountered during the simulations. The 2D VAT model proved particularly sensitive to convergence, requiring the consolidation phases to be applied in very small time increments and load fraction factors and increased iteration and step limits, to reduce the risk of kernel errors during simulation. This sensitivity is a direct consequence of combining two advanced nonlinear constitutive models within the VAT framework, which amplifies the complexity of the incremental-iterative solution.

The 3D MNHard simulations encountered solver convergence issues related to mesh quality and solver type compatibility. Switching solvers and applying some of the same practices that was found to help the VAT simulations usually worked, however, at the cost of substantially longer computation time. The mesh sensitivity analysis confirmed convergence at approximately 20 000 nodes for the Concrete Model, beyond which further refinement yielded negligible change in total settlement. Coarser mesh underestimated the settlements by approximately 1 cm, which is modest in absolute terms but represents non-conservative result in the context of relatively small predicted total settlements.

8

Conclusion

This thesis investigated the numerical modeling of lime-cement column reinforced embankments using PLAXIS 2D and 3D, with a focus on the Volume Averaging Technique (VAT) as well as alternative constitutive models for the columns. The numerical simulations for the case in Nödinge were compared against measured settlement and pore pressure data available and complemented by hand calculations following the Swedish design method. The comparison between the column models was aimed solely at evaluating how the settlement behavior was captured when modeling the same columns using different modeling approaches.

8.1 Volume Averaging technique (VAT)

The hand calculations resulted in a total Green Field settlement of 1.74 m, with full consolidation requiring approximately 160 years. After LCC reinforcement, the settlements were reduced to approximately 0.06-0.07 meters after 20 years, excluding creep, in close agreement with the reference project and the field measurements. These results confirm that the Swedish method remains a reliable baseline for settlement estimate in LCC-reinforced soil.

Followed by the hand calculations, the test embankment in Nödinge was modeled using VAT in 2D and also set to comparison with the same material models in 3D. The study confirmed that the VAT is a practical and sufficiently accurate tool for SLS serviceability analyses of LCC-reinforced embankments. The VAT successfully captured the overall settlement behavior of the embankment. The immediate settlement response at each loading stage and the consolidation behavior between the two construction phases were both decently well represented. The simulated settlement response is between the measured column and soil settlements, as expected from a homogenization approach in which both components contribute to a single equivalent material response.

Slight variations from the measured data were concluded to be partly due to uncertainties in the input parameters, such as the clay modulus and permeability, as well as similar uncertainties in the column properties, all resulting from insufficient laboratory data. Additional variations in the pore pressure dissipation behavior were attributed to the "wished-in-place" assumption, which neglects the installation induced excess pore pressures in the numerical simulations, despite these being present in the in-situ measurements.

Another observation from the simulations was the underestimation of the differential settlements between the columns and the surrounding soil. The kinematic compatibility constraint, which is part of the VAT formulation, enforces equal vertical strains in the columns and the soil through the assumption of perfect bonding. While the measured data generally confirmed this assumption throughout most of the stabilized block, some local differences between column and soil settlements were still observed due to arching effects at the very top of the measured values. The main differences between the measured and simulated differential settlements are also attributed to these arching effects and the transition zone, which was not fully captured in the numerical simulations. It is therefore good that the VAT simulations were more closely aligned to the measured column settlement, as the soil settlement at the very top is not a good representative due to the arching effect.

After conducting the same simulations with the same material models in a 3D setting, the results supported the claim that VAT is a simplification of a 3D problem into a 2D formulation while maintaining comparable accuracy. The simulated settlement versus depth was, if not identical, very similar to the 3D results. However, the arching effects in the transition zones were included and better captured in the 3D simulations of course and not in VAT.

8.2 Comparison of Constitutive Models

Among the column models, The MNHard model, used for the columns in both the VAT (2D) and 3D simulations with undrained drainage conditions, produced the best overall agreement with the field-measured settlement data. The Concrete Model, however, showed strong potential to capture several aspects of column behavior. Its principal advantage over MNHard is its ability to simulate both strain-induced hardening and softening, ductility, creep, as well as a clearly defined failure and residual strength, making it potentially more informative for ULS analyses. The Soil Test calibration confirmed that the Concrete Model reproduced the stress-strain response with good accuracy, and in this respect outperforms MNHard in matching the triaxial test curve for Type B parameters. but appears to be more suitable for ULS analyses.

In this study however, the simulated settlements were highly dependent on the drainage assumptions, and for the same material properties different settlement behaviors were obtained. In reality, the columns behave under undrained conditions, whereas the Concrete Model can only be represented as either drained or non-porous. Whether one formulation is more reliable could not be assessed in this thesis due to a lack of settlement measurements. Therefore the formulated aim with an interest of being able to model LC-columns less conservatively remains of interest. However, the analysis conducted here can serve as a basis for further investigation of the model and its applicability to serviceability limit state analyses in LCC-reinforced soils.

8.3 Suggestions for Further Work

There are multiple aspects found during this study that could not be explored more thoroughly due to time constraints. These are instead chosen to be suggestions for further work. The most significant improvement would be finding a robust link between VAT and the Swedish design method. In this thesis, this aspect was examined by investigating whether the elasto-plastic zone definition in the Swedish method could be represented within VAT by identifying failure and yielding mechanisms within the material models and components. The results revealed that this consideration requires further investigation and represents a potential for future development of the VAT approach. The VAT code could be modified to include the plastic point definitions that are currently missing. In addition, a more detailed analysis of deformation mechanisms and an investigation into the applicability of VAT for ULS analyses remain of interest.

For floating columns, as in the case of this thesis, creep in the underlying soil can have a significant influence when the time period is increased. At the time of this study, numerical limitations associated with combining multiple complex material models made it impractical to include creep effects. However, it is a potential suggestion for further improvement in future investigations using the VAT approach. This could be achieved by implementing an improved variant of the S-CLAY1S model, such as the Creep-SCLAY1S model in the underlying and surrounding soil. Implementing Creep-SCLAY1S in the VAT model itself would require another constitutive model for the columns as well that can also utilize a creep formulation.

When it comes to the Concrete Model, the implementation of an undrained formulation in PLAXIS would enable a more direct comparison with the MNHard model under equivalent drainage conditions. Another aspect that would improve the comparison between the two models is the availability of a reference site with measured settlement data as well as more comprehensive data on the column properties. This would ideally include both triaxial compression and tension tests extended to failure for the columns, alongside the other parameters already available in this thesis.

Besides the drainage type, a coupled hydro-mechanical analysis that accounts for installation-induced pore pressures would also improve the initial conditions of the simulations and reduce the offset observed in the early pore pressure response.

Bibliography

Helen Åhnberg & Göran Holm. (1986). *Rapport No 31, Kalkpelarmetoden.* Swedish Geotechnical Institute.

Gens, A., & Nova, A. (1993). Conceptual bases for a constitutive model for bonded soils and weak rocks. *Proc., Int. Symp. on Geotechnical Engineering of Hard Soils-Soft Rocks.*

Carlsten, P., & Swedish Geotechnical Institute. (1996). Lime and Lime/Cement Columns. *Developments in Geotechnical engineering*, *Volume 80*, 355–399. https://doi.org/10.1

Terzaghi, K., Peck, R. B., & Mesri, G. (1996). *Soil Mechanics in Engineering Practice* (3rd).

Edstam Torbjörn & Swedish Deep Stabilization Research Centre. (1997). *Erfarenhetsbank för kalk-cementpelare, Rapport 1* (tech. rep.).

Baker, S. (2000). *Deformation behavior of lime/cement column stabilized clay.* Dept. of Geotechnical Engineering, Chalmers University of Technology.

Wheeler, S. J., Näätänen, A., Karstunen, M., & Lojander, M. (2003). An anisotropic elastoplastic model for soft clays. *Canadian Geotechnical Journal*, *40*(2), 403–418. https://doi.org/10.1139/t02-119

Broms, B. B. (2004). *Lime and lime/cement columns* (tech. rep.).

European Committee For Standardization. (2004, November). *EN 1997 Eurocode 7: Geotechnical design* (tech. rep.).

Alén, C., Baker, S., Bengtsson, P.-E., & Sällfors, G. (2005). Lime/Cement Column Stabilised Soil -A New Model for Settlement Calculation. *Deep Mixing.*

Karstunen, M., Krenn, H., Simon, ; Wheeler, J., Koskinen, M., & Zentar, R. (2005). Effect of Anisotropy and Destructuration on the Behavior of Murro Test Embankment. https://doi.org/10.1061/ASCE1532-364120055:287

Karstunen, M., Krenn, H., & Vogler, U. (2006). Numerical Modelling of deep mixing by volume averaging technique. In *Numerical methods in geotechnical engineering* (pp. 793–799). Taylor & Francis.

Karstunen, M., Wiltafsky, C., Krenn, H., Scharinger, F., & Schweiger, H. F. (2006). Modelling the behaviour of an embankment on soft clay with different constitutive models. *International Journal for Numerical and Analytical Methods in Geomechanics*, *30*(10), 953–982. https://doi.org/10.1002/nag.507

Swedish Deep Stabilization Research Centre, Alén, C., Sällfors, G., Bengtsson, E., & Baker, S. (2006). *Rapport 15 Provbankar Riksväg 45/Nordlänken Bankar på kalkcementpelarförstärkt jord-Beräkningsmodell för sättningar* (tech. rep.). www.swedgeo.se/sd.

Swedish Deep Stabilization Research Centre & Larsson, R. (2006). *Rapport 17 Djupstabilisering med bindemedels-stabiliserade pelare och masstabilisering-En vägledning* (tech. rep.). www.swedgeo.se.

Benz, T. (2007). *Small-Strain Stiffness of Soils and its Numerical Consequences* [Doctoral dissertation, Insitute of Geotechnics - University of Stuttgart].

Edstam, T. (2007). Provbankar, Väg 45. *KC-pelardagar*.

Vogler, U. (2008, September). *Numerical Modelling of Deep Mixing with Volume Averaging Technique* [Doctoral dissertation, University of Strathclyde].

Alén, C. (2009). *Appendix B - LCC stabilized soil - Extent of and stresses in the plastic zone/zone A* (tech. rep.).

Alén, C. (2012). *On Consolidation of Lime/Cement columns: Appendix C* (tech. rep.).

Sällfors, G., & Alén, C. (2012). *Geotechnics: Lime/Cement Columns* (tech. rep.).

Sällfors, G. (2013). Geoteknik.

Becker, P., & Karstunen, M. (2014). VOLUME AVERAGING TECHNIQUE FOR MODELLING DEFORMATIONS IN SOFT SOIL IMPROVED WITH DEEP MIXED COLUMNS. *International Conference on Piling and Deep Foundations*.

Than, S. T., & Anantanasakul, P. (2023, May). *Study on the Application of the Concrete Model in PLAXIS to Bangkok Clay improved with Portland Cement* (tech. rep.). Phuket.

Jonsson, C. (2024, February). Keller: Att välja Jordförstärkningsteknik. https://chalmers.instructure.com/courses/27818/files/3273128?module_item_id=448672

Larsson Stefan. (2025). *Reviderad beräkningsmodell KC-pelare - möjligheter, TRV 2024/113470* (tech. rep.). KTH Royal Institute of Technology. https://www.byv.kth.se/en/forskning8/pagaende-forskningsp/jord-och-bergmekani/forskning-jord-och-bergmekanik/reviderad-berakningsmodell-kc-pelare-mojligheter-trv-2024-113470-1.1418728

Seequent. (2025, September). *PLAXIS 3D 2025.1 Materials Models Manual* (tech. rep.).

Abed, A., Vogler, U., & Karstunen, M. (2026). Volume Averaging Technique for Deep-Mixed Columns under Embankments: Verification and Validation. *International Journal of Geomechanics*, *26*(1). https://doi.org/10.1061/ijgnai.gmeng-11450

Edstam, T. (2026). Private conversation.

Karstunen, M., & Koskinen, M. (n.d.). Plastic anisotropy of soft reconstituted clays.

WSP/BohusGeo. (n.d.). CRS Tests Nordlänken.

A
CRS Data

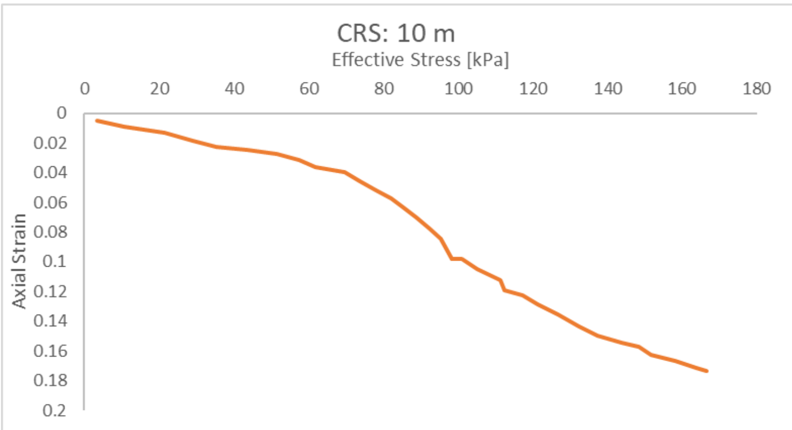

Figure A.1: Data extracted from provided CRS test at 10 meters depth

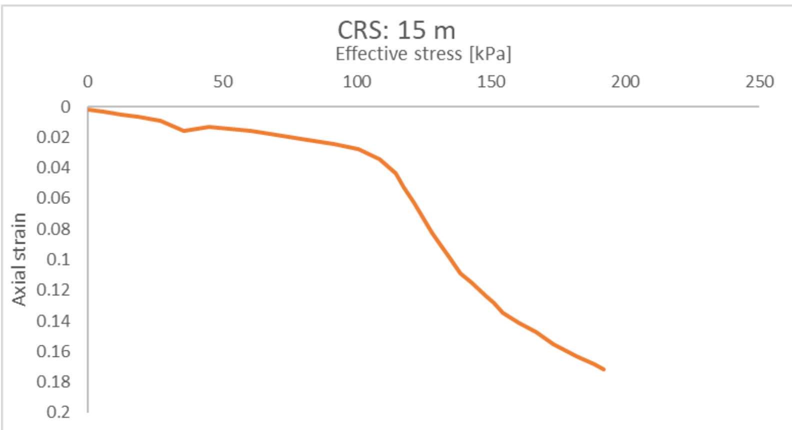

Figure A.2: Data extracted from provided CRS test at 15 meters depth

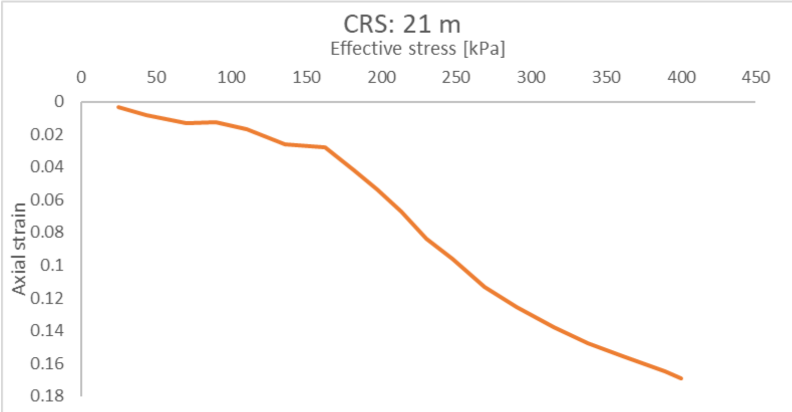

Figure A.3: Data extracted from provided CRS test at 21 meters depth

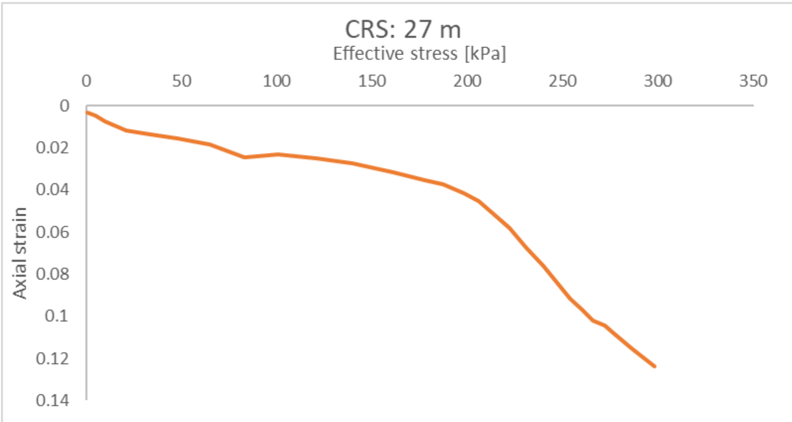

Figure A.4: Data extracted from provided CRS test at 27 meters depth

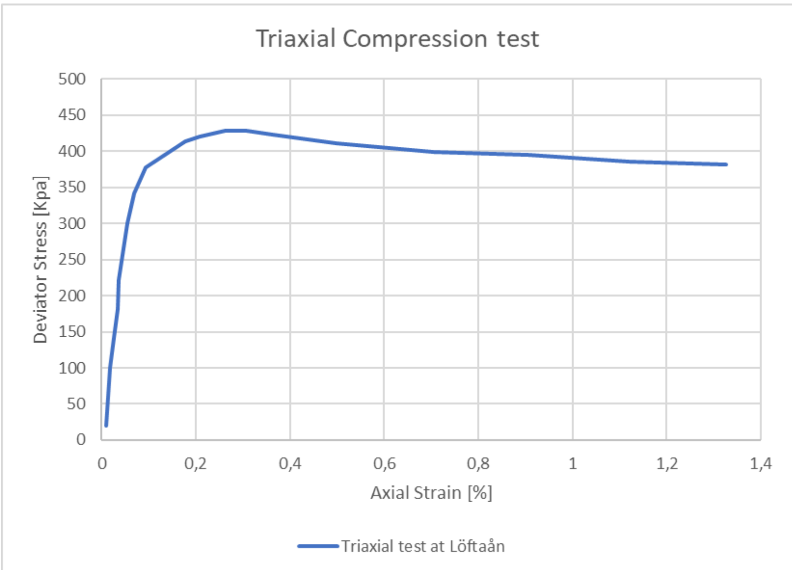

Figure A.5: Results of triaxial compression test at 20 kpa confining pressure (Baker, 2000)

B

Creep Settlements

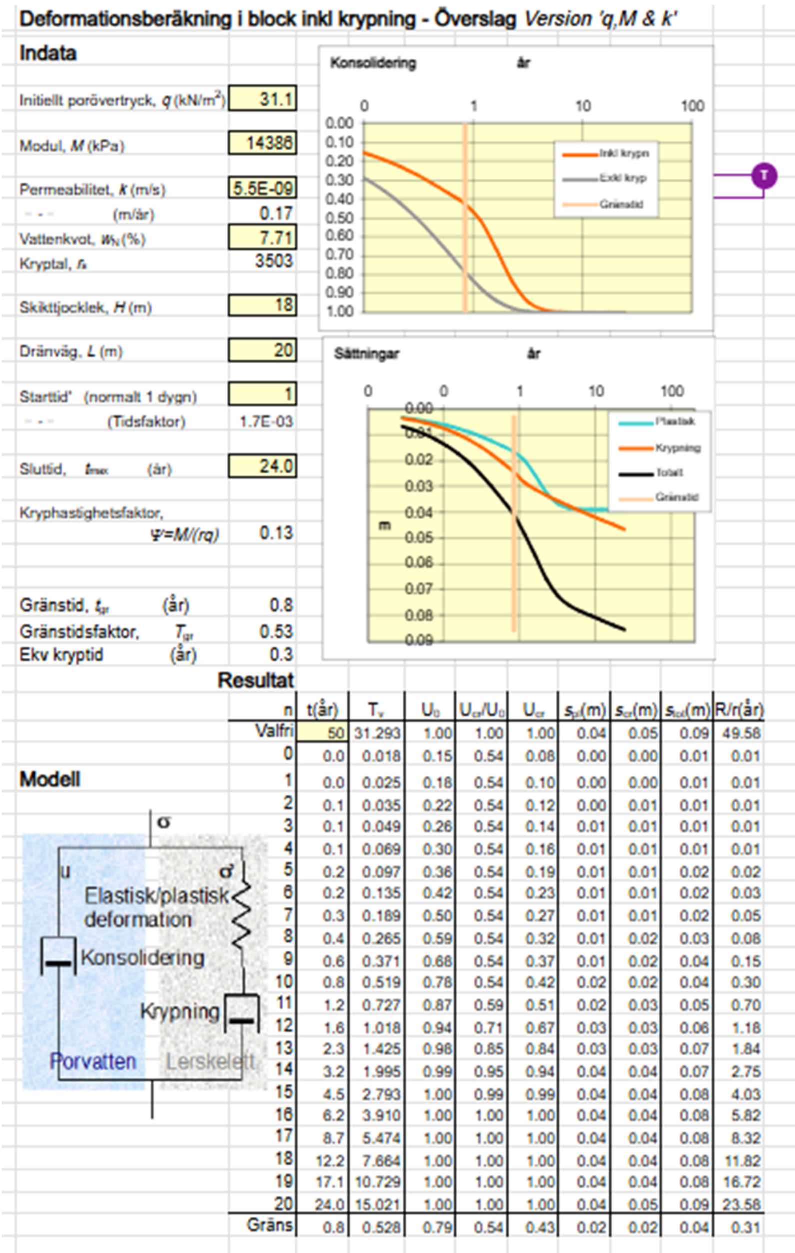

Deformationsberäkning i block inkl krypning - Överslag *Version 'q,M & k'*

Indata

Initiellt poröverttryck, q (kN/m^2)	31.1
Modul, M (kPa)	14386
Permeabilitet, k (m/s)	5.5E-09
- - - (m/år)	0.17
Vattenkvot, w_N (%)	7.71
Kryptal, r_s	3503
Skikttjocklek, H (m)	18
Dränväg, L (m)	20
Starttid' (normalt 1 dygn)	1
- - - (Tidsfaktor)	1.7E-03
Sluttid, t_{max} (år)	24.0
Kryphastighetsfaktor, $\Psi = M/(rq)$	0.13
Gränstid, t_{gr} (år)	0.8
Gränstidsfaktor, T_{gr}	0.53
Ekv kryptid (år)	0.3

Resultat

n	t(år)	T_v	U_0	U_{cr}/U_0	U_{cr}	s_{pl}(m)	s_{cr}(m)	s_{tot}(m)	R/r(år)
Valfri	50	31.293	1.00	1.00	1.00	0.04	0.05	0.09	49.58
0	0.0	0.018	0.15	0.54	0.08	0.00	0.00	0.01	0.01
1	0.0	0.025	0.18	0.54	0.10	0.00	0.00	0.01	0.01
2	0.1	0.035	0.22	0.54	0.12	0.00	0.01	0.01	0.01
3	0.1	0.049	0.26	0.54	0.14	0.01	0.01	0.01	0.01
4	0.1	0.069	0.30	0.54	0.16	0.01	0.01	0.01	0.01
5	0.2	0.097	0.36	0.54	0.19	0.01	0.01	0.02	0.02
6	0.2	0.135	0.42	0.54	0.23	0.01	0.01	0.02	0.03
7	0.3	0.189	0.50	0.54	0.27	0.01	0.01	0.02	0.05
8	0.4	0.265	0.59	0.54	0.32	0.01	0.02	0.03	0.08
9	0.6	0.371	0.68	0.54	0.37	0.01	0.02	0.04	0.15
10	0.8	0.519	0.78	0.54	0.42	0.02	0.02	0.04	0.30
11	1.2	0.727	0.87	0.59	0.51	0.02	0.03	0.05	0.70
12	1.6	1.018	0.94	0.71	0.67	0.03	0.03	0.06	1.18
13	2.3	1.425	0.98	0.85	0.84	0.03	0.03	0.07	1.84
14	3.2	1.995	0.99	0.95	0.94	0.04	0.04	0.07	2.75
15	4.5	2.793	1.00	0.99	0.99	0.04	0.04	0.08	4.03
16	6.2	3.910	1.00	1.00	1.00	0.04	0.04	0.08	5.82
17	8.7	5.474	1.00	1.00	1.00	0.04	0.04	0.08	8.32
18	12.2	7.664	1.00	1.00	1.00	0.04	0.04	0.08	11.82
19	17.1	10.729	1.00	1.00	1.00	0.04	0.04	0.08	16.72
20	24.0	15.021	1.00	1.00	1.00	0.04	0.05	0.09	23.58
Gräns	0.8	0.528	0.79	0.54	0.43	0.02	0.02	0.04	0.31

Modell

Figure B.1: Calculated creep settlements for the stabilized block

Deformationsberäkning i lera inkl krypning - Överslag *Version 'q,M & k'*

Indata

Initiellt porövertryck, q (kN/m^2)	13.5
Modul, M (kPa)	7941.3
Permeabilitet, k (m/s)	9.0E-10
- - - (m/år)	0.03
Vattenkvot, w_N (%)	29
Kryptal, r_s	480
Skikttjocklek, H (m)	15
Dränväg, L (m)	10
Starttid' (normalt 1 dygn)	1
- - - (Tidsfaktor)	6.1E-04
Sluttid, t_{max} (år)	24.0
Kryphastighetsfaktor,	*Varning !*
$\Psi = M/(rq)$	1.22
Modellen utvärderad för	$\Psi < 0{,}3$
Gränstid, t_{gr} (år)	21.8
Gränstidsfaktor, T_{gr}	4.90
Ekv kryptid (år)	8.0

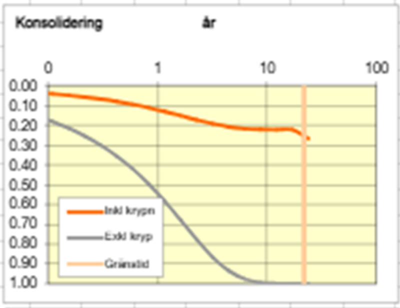

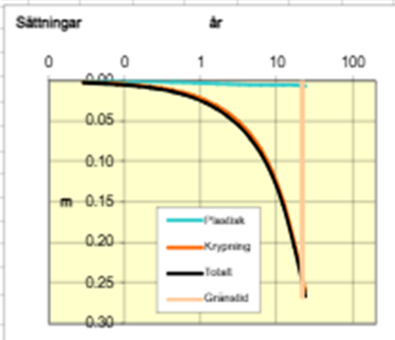

Resultat

n	t(år)	T_v	U_0	U_{cr}/U_0	U_{cr}	s_{pl}(m)	s_{cr}(m)	s_{tot}(m)	R/r(år)
Valfri	50	11.215	1.00	0.86	0.86	0.02	0.30	0.32	38.56
0	0.0	0.006	0.09	0.22	0.02	0.00	0.00	0.00	0.00
1	0.0	0.009	0.11	0.22	0.02	0.00	0.00	0.00	0.00
2	0.1	0.013	0.13	0.22	0.03	0.00	0.00	0.00	0.00
3	0.1	0.018	0.15	0.22	0.03	0.00	0.00	0.00	0.00
4	0.1	0.025	0.18	0.22	0.04	0.00	0.00	0.01	0.00
5	0.2	0.035	0.21	0.22	0.05	0.00	0.01	0.01	0.00
6	0.2	0.048	0.25	0.22	0.06	0.00	0.01	0.01	0.00
7	0.3	0.068	0.30	0.22	0.07	0.00	0.01	0.01	0.00
8	0.4	0.095	0.35	0.22	0.08	0.00	0.01	0.01	0.00
9	0.6	0.133	0.42	0.22	0.09	0.00	0.01	0.02	0.00
10	0.8	0.186	0.50	0.22	0.11	0.00	0.02	0.02	0.01
11	1.2	0.261	0.58	0.22	0.13	0.00	0.02	0.03	0.01
12	1.6	0.365	0.68	0.22	0.15	0.00	0.03	0.03	0.01
13	2.3	0.511	0.78	0.22	0.17	0.00	0.04	0.04	0.01
14	3.2	0.715	0.87	0.22	0.19	0.00	0.05	0.06	0.01
15	4.5	1.001	0.93	0.22	0.21	0.01	0.07	0.07	0.02
16	6.2	1.401	0.98	0.22	0.22	0.01	0.09	0.09	0.04
17	8.7	1.962	0.99	0.22	0.22	0.01	0.11	0.12	0.10
18	12.2	2.747	1.00	0.22	0.22	0.01	0.15	0.15	0.32
19	17.1	3.845	1.00	0.22	0.22	0.01	0.20	0.21	1.65
20	24.0	5.383	1.00	0.27	0.27	0.01	0.26	0.27	11.20
Gräns	21.8	4.899	1.00	0.23	0.23	0.01	0.25	0.26	8.04

Modell

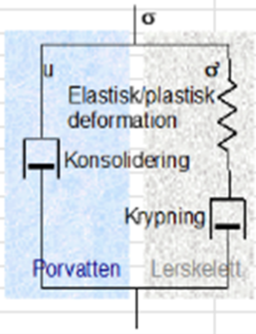

Figure B.2: Calculated creep settlements for the underlying clay

C

Material Parameters

Table C.1: Material Parameters for S-CLAY1S Model before Soil Test - Type A

Parameter	Descriptor	2–12 m	12–20 m	Underlying clay	Unit
γ	Unit Weight	14.6	15.3	16	$[kN/m^3]$
κ	Swelling index	0.04	0.02	0.02	[-]
ν	Poisson's ratio	0.2	0.2	0.2	[-]
λ	Compression index	0.21	0.18	0.21	[-]
M	Stress ratio at the critical state in triaxial compression	1.2	1.2	1.2	[-]
ω	Absolute rate of rotational hardening	73	85	71	[-]
ω_d	Relative rate of rotational hardening due to deviatoric strain	0.76	0.76	0.76	[-]
ξ	Absolute rate of destructuration	8	8	8	[-]
ξ_d	Relative rate of destructuration due to deviatoric strain	0.5	0.5	0.2	[-]
POP	Pre Overburden Pressure	-7.7	-17.5	-32.5	[kPa]
e_0	Initial void ratio	2.49	2.1	1.7	[-]
α_0	Initial inclination of the yield surface	0.4575	0.4575	0.4575	[-]
x_0	Initial bonding parameter	15	15	15	[-]
k	Permeability	8.64E-05	8.64E-05	8.64E-05	[m/day]

Table C.2: Material Parameters for S-CLAY1S Model After soil Test

Parameter	Descriptor	2–12 m	12–20 m	Underlying clay	Unit
γ	Unit Weight	14.6	15.3	16	$[kN/m^3]$
κ	Swelling index	0.05	0.05	0.03	[-]
ν	Poisson's ratio	0.2	0.2	0.2	[-]
γ	Compression index	0.215	0.25	0.22	[-]
M	Stress ratio at the critical state in triaxial compression	1.2	1.2	1.2	[-]
ω	Absolute rate of rotational hardening	73	50	50	[-]
ω_d	Relative rate of rotational hardening due to deviatoric strain	0.76	0.76	0.75	[-]
ξ	Absolute rate of destructuration	8	8	8	[-]
ξ_d	Relative rate of destructuration due to deviatoric strain	0.5	0.5	0.2	[-]
POP	Pre Overburden Pressure	-7.7	-17.5	-32.5	[kPa]
e_0	Initial void ratio	2.49	2.1	1.7	[-]
α_0	Initial inclination of the yield surface	0.4575	0.4575	0.4575	[-]
x_0	Initial bonding parameter	15	15	15	[-]
k	Permeability	8.64E-05	8.64E-05	8.64E-05	[m/day]

Table C.3: Material Parameters for MNHard Model before Soil Test - Type A

Parameter	Descriptor	Value (2–12 m)	Value (12–20 m)	Unit
γ	Unit Weight	14.6	15.3	$[kN/m^3]$
G_{ref}	Reference shear modulus	229	229	[MPa]
ν	Poisson's ratio	0.33	0.33	[-]
ϕ_{max}	Maximum friction angle	35	35	[°]
C_{ref}	Cohesion	75	75	[kPa]
ψ	Dilatancy angle	0	0	[°]
m	Power of Hyperbolic stress-strain law	0.7	0.7	[-]
p_{ref}	Reference pressure for hyperbolic stress-strain law	100	100	[kPa]
R_f	Ratio of failure	0.9	0.9	[-]
G_{50}	Shear modulus for primary loading	76200	76200	[kPa]
k	Permeability	4.48E-04	4.48E-04	[m/day]

Table C.4: Material Parameters for MNHard Model after Soil Test - Type B

Parameter	Descriptor	Value (2–12 m)	Value (12–20 m)	Unit
γ	Unit Weight	14.6	15.3	$[kN/m^3]$
G_{ref}	Reference shear modulus	400	400	[MPa]
ν	Poisson's ratio	0.33	0.33	[-]
ϕ_{max}	Maximum friction angle	35	35	[°]
C_{ref}	Cohesion	90	90	[kPa]
ψ	Dilatancy angle	0	0	[°]
m	Power of Hyperbolic stress-strain law	0.7	0.7	[-]
p_{ref}	Reference pressure for hyperbolic stress-strain law	100	100	[kPa]
R_f	Ratio of failure	0.9	0.9	[-]
G_{50}	Shear modulus for primary loading	300	300	[MPa]
k	Permeability	4.48E-04	4.48E-04	[m/day]

Table C.5: Material Parameters for concrete Model - Type A

Parameter	Descriptor	Value (2–12 m)	Value (12–20 m)	Unit
γ	Unit Weight	14.6	15.3	$[kN/m^3]$
E_{28}	Young's modulus after 28 days	291.2	291.2	[MPa]
ν	Poisson's ratio	0.33	0.33	[-]
$f_{c,28}$	Uniaxial compressive strength after 28 days	390	546	[kPa]
f_{c0n}	Normalized initial yield strength in compression	0.5038	0.5038	[-]
f_{cfn}	Normalized failure strength in compression	0.4955	0.4955	[-]
f_{cun}	Normalized residual strength in compression	0.4955	0.4955	[-]
$G_{c,28}$	Compressive fracture energy after 28 days	10	10	[kN/m]
ϕ_{max}	Maximum friction angle	30.95	30.95	[°]
ψ	Dilancy angle	3.412	3.412	[°]
γ_{fc}	Safety factor for compressive strength	1	1	[-]
$f_{t,28}$	Uniaxial tensile strength after 28 days	53.4	53.4	[kPa]
f_{tun}	Normalized residual strength in tension	0.001	0.001	[-]
$G_{t,28}$	Tensile fracture energy after 28 days	0.005	0.005	[kN/m]
γ_{ft}	Safety factor for tensile strength	1	1	[-]
ϵ^p_{cp}	Plastic peak strain in uniaxial compression	-0.002443	-0.002443	[-]
a_{duct}	Increase of ϵ^p_{cp} with confining pressure	9.58	9.58	[-]
k	Permeability	-	-	[m/day]

Table C.6: Material Parameters for concrete Model - Type B

Parameter	Descriptor	Value (2–12 m)	Value (12–20 m)	Unit
γ	Unit Weight	14.6	15.3	$[kN/m^3]$
E_{28}	Young's modulus after 28 days	450	450	[MPa]
ν	Poisson's ratio	0.33	0.33	[-]
$f_{c,28}$	Uniaxial compressive strength after 28 days	390	514	[kPa]
f_{c0n}	Normalized initial yield strength in compression	0.85	0.85	[-]
f_{cfn}	Normalized failure strength in compression	0.55	0.55	[-]
f_{cun}	Normalized residual strength in compression	0.30	0.30	[-]
$G_{c,28}$	Compressive fracture energy after 28 days	8	8	[kN/m]
ϕ_{max}	Maximum friction angle	30	30	[°]
ψ	Dilatancy angle	0	0	[°]
γ_{fc}	Safety factor for compressive strength	1	1	[-]
$f_{t,28}$	Uniaxial tensile strength after 28 days	43	57	[kPa]
f_{tun}	Normalized residual strength in tension	0.001	0.001	[-]
$G_{t,28}$	Tensile fracture energy after 28 days	0.005	0.005	[kN/m]
γ_{ft}	Safety factor for tensile strength	1	1	[-]
ϵ^p_{cp}	Plastic peak strain in uniaxial compression	-0.002	-0.002	[-]
a_{duct}	Increase of ϵ^p_{cp} with confining pressure	1	1	[-]
k	Permeability	-	-	[m/day]

DEPARTMENT OF SOME SUBJECT OR TECHNOLOGY
CHALMERS UNIVERSITY OF TECHNOLOGY
Gothenburg, Sweden
www.chalmers.se

CHALMERS
UNIVERSITY OF TECHNOLOGY